North Carolina Agricultural and Technical State University
Aggie Digital Collections and Scholarship

Theses | Electronic Theses and Dissertations

2011

A Study Of Magnesium Oxide Biodegradable Coatings For Magnesium-Based Implants.

Ashlyn N. Worthy
North Carolina Agricultural and Technical State University

Follow this and additional works at: https://digital.library.ncat.edu/theses

Recommended Citation

Worthy, Ashlyn N., "A Study Of Magnesium Oxide Biodegradable Coatings For Magnesium-Based Implants." (2011). *Theses*. 48.
https://digital.library.ncat.edu/theses/48

This Thesis is brought to you for free and open access by the Electronic Theses and Dissertations at Aggie Digital Collections and Scholarship. It has been accepted for inclusion in Theses by an authorized administrator of Aggie Digital Collections and Scholarship. For more information, please contact iyanna@ncat.edu.

A STUDY OF MAGNESIUM OXIDE BIODEGRADABLE COATINGS FOR MAGNESIUM-BASED IMPLANTS

by

Ashlyn N. Worthy

A thesis submitted to the graduate faculty
in partial fulfillment of the requirements for the degree of
MASTER OF SCIENCE

Department: Mechanical Engineering
Major: Mechanical Engineering
Major Professor: Dr. Jagannathan Sankar

North Carolina A&T State University
Greensboro, North Carolina
2011

School of Graduate Studies
North Carolina Agricultural and Technical State University

This is to certify that the Master's Thesis of

Ashlyn N. Worthy

has met the thesis requirements of
North Carolina Agricultural and Technical State University

Greensboro, North Carolina
2011

Approved by:

_____	_____
Dr. Jagannathan Sankar Major Professor	Dr. Sergey Yarmolenko Committee Member
_____	_____
Dr. Devdas Pai Committee Member	Dr. Yeoheung Yun Committee Member
_____	_____
Dr. Samuel P. Owusu-Ofori Department Chairperson	Dr. Sanjiv Sarin Associate Vice Chancellor for Research and Graduate Dean

DEDICATION

This thesis is dedicated to my loving mother, Charlene Lewis Worthy. Thank you so much for your support and encouragement throughout my life and ESPECIALLY through the completion of my graduate school work. I love you so much and I thank God every day for blessing me with such a wonderful mother. **I LOVE YOU!!!!!!**

BIOGRAPHICAL SKETCH

Ashlyn N. Worthy was born on October 14, 1986 in Atlanta, Georgia. She received a Bachelor of Science degree in Mechanical Engineering, with honors, from North Carolina Agricultural and Technical State University in May 2009. As an undergraduate student, Ashlyn was a member of the Honors Program, Pi Tau Sigma International Mechanical Engineering Honor Society, Tau Beta Pi Engineering Honor Society, Golden Key Honor Society, Alpha Lambda Delta Honor Society, Alpha Kappa Alpha Sorority, Incorporated and the Dean's List. Her professional experience includes three summer internships with three different companies: Georgia Power, Honda of America Manufacturing, Inc. and Cummins, Inc. Ashlyn joined the Master of Science program in Mechanical Engineering at North Carolina Agricultural and Technical State University in August of 2009. She worked as a teaching assistant in the Department of Mechanical Engineering during the 2009-2010 school year and as a research assistant for the National Science Foundation Engineering Research Center for Revolutionizing Metallic Biomaterials from the summer of 2010 until the completion of the degree requirements.

ACKNOWLEDGMENTS

First and foremost, I would like to acknowledge my Lord and Savior Jesus Christ for being with me through this demanding graduate school journey. If it wasn't for Him constantly having my back, I would have quit this graduate school journey a long time ago. I thank Him for giving me the strength and courage to be able to see this journey through to the end and for allowing me to learn so many valuable lessons along the way. I love you Lord and thank You so much for keeping me through this journey. I can't wait to see what You have planned for me next! The best is yet to come!

I would like to acknowledge my advisor Dr. Jagannathan Sankar for giving me the opportunity to participate in the National Science Foundation Engineering Research Center (ERC) for Revolutionizing Metallic Biomaterials. Being a part of the ERC has been a wonderful opportunity and it has opened my eyes to the many opportunities that are available in the Mechanical Engineering field. I would like to acknowledge my co-advisor Dr. Sergey Yarmolenko for guiding me through my daily research activities, for teaching me how to be an efficient researcher and for helping me to understand how to analyze data. Thank you for being dedicated to my research and I truly appreciate all the guidance that I received from you. I would like to acknowledge Dr. John Kizito for believing I had the capability and the intelligence to pursue a graduate degree and for encouraging me to stay in school after I received my Bachelor's degree. I would like to acknowledge Dr. Devdas Pai for taking time out of his busy schedule to read over my thesis and ensuring that it was free of grammatical errors. I would like to acknowledge

Dr. Samuel Owusu-Ofori for looking over my thesis and making sure that it was properly formatted.

Mr. Ruben Kotoka, thank you for being an excellent mentor, for teaching me how to use the lab equipment and for being there whenever I needed some assistance in the lab. Ms. Erica Clinard, thank you for assisting in the completion of my experiments. Ms. Svitlana Fialkova, thank you for being willing to answer any questions that I may have had and for showing me how to use the equipment in the lab. Dr. Zhigang Xu, thank you for helping me with operating the SEM. Dr. Seonghyuk Ko, thank you for helping me with my electrochemical work. Dr. Jenora Waterman, thank you for working with me to develop biological tests for the completion of my research and for allowing me to use your lab to perform biological tests on my materials. Ms. Christa Watson, thank you for working with me to develop biological tests, for teaching me how to work with cells and for the training that I received from you.

Last, but not least, I want to express my appreciation to my labmates Leon White, Christopher Smith and Christopher Mahoney. Thank you all so much for the laughs and encouragement and for making my graduate school journey a little easier to handle.

TABLE OF CONTENTS

LIST OF FIGURES

FIGURE **PAGE**

LIST OF TABLES

NOMENCLATURE AND SYMBOLS

AC Alternating Current

ATCC American Type Culture Collection

Cu Copper

CVD Chemical Vapor Deposition

DC Direct Current

DMSO Dimethyl sulfoxide

DPBS Dulbecco's Phosphate-Buffered Saline

EDS Energy-dispersive X-ray Spectroscopy

EDTA Ethylenediaminetetraacetic acid

FBS Fetal Bovine Serum

HBSS Hank’s Balanced Salt Solutions

Mg Magnesium

MgO Magnesium Oxide

mT Millitorr

PBS Phosphate Buffered Saline

PDC Pulsed Direct Current

PVD Physical Vapor Deposition

NCAT North Carolina Agricultural and Technical State University

RF Radio Frequency

RGA Residual Gas Analyzer

sccm Standard Cubic Centimeters per Minute

SE Secondary Electron

SEM Scanning Electron Microscope

XRD X-ray Diffraction

XRR X-ray Reflectometry

ABSTRACT

Worthy, Ashlyn N. A STUDY OF MAGNESIUM OXIDE BIODEGRADABLE COATINGS FOR MAGNESIUM-BASED IMPLANTS. (**Major Advisors: Dr. Jagannathan Sankar and Dr. Sergey Yarmolenko),** North Carolina Agricultural and Technical State University.

Magnesium (Mg) and its alloys are great candidates for uses in orthopedic implant applications due to their biocompatibility, mechanical properties and degradability. However, Mg and its alloys are susceptible to accelerated degradation rates due to galvanic corrosion, which leads to unpredictable corrosion behavior. The objective of this study is to develop biocompatible, functional thin film magnesium oxide (MgO) coatings that: (1) serve as a galvanic separator between metallic substrates and metallic coatings, (2) control the rate of corrosion of Mg-based implants, (3) have controlled resorption times based on coating thickness, (4) promote osseointegration and (5) are predictable in corrosive environments.

An Mg screw was coated with copper (Cu) using direct current (DC) magnetron sputtering and galvanic corrosion was observed from the direct contact of the metallic substrate and metallic coating. MgO thin films were developed, to serve as an intermediate layer, using pulsed DC reactive magnetron sputtering. The sputtering of MgO was optimized through oxygen content, frequency and power. Multilayered Mg-MgO-Cu and Mg-MgO systems were created and individual layer thicknesses were measured using X-ray reflectometry (XRR) analysis software. Immersion tests were performed on Mg-MgO systems with varying thicknesses using the optical density

method. The tests were performed at room temperature with deionized water and phosphate buffered saline (PBS) and were also done at 37ºC with albumin, media, media with fetal bovine serum (FBS), saline and PBS. The results were used to calculate resorption times and this information was used to perform a cell adhesion assay. This study shows that MgO exhibited biocompatibility, controlled the rate of Mg corrosion and is a good candidate for a galvanic separator material.

CHAPTER 1

INTRODUCTION

1.1 Overview

A critical part in metallic biomaterials advances is the surface engineering of metallic implants because it addresses processes on the interface between the implant and the surrounding tissue. The success of new materials development for degradable as well as permanent implants is oftentimes dependent upon interface properties and interfacial properties. Corrosion properties of implant materials depend on structure as well as composition of the alloy. The same composition in single crystal, amorphous or polycrystalline can have considerably different corrosion properties. Since most metallurgical processing methods inevitably lead to small amounts of uncontrollable impurities, the main source of unpredictable corrosion behavior of metallic alloys, where contact between the grains of different phases and impurities increases pitting corrosion, is inhomogeneity. A promising solution for metallic implant surface modification with controlled corrosion is the application of coatings from pure components. Galvanic potentials between grains, which is the main source of electrochemical corrosion, can be eliminated through the development of amorphous coatings. These amorphous coatings can open up new types of biocompatible, Mg-based, slow degrading metallic coatings. Galvanic effects can also be controlled through the deposition of dielectric separators between metallic substrates and metallic coatings.

For both degradable and permanent implants the role of coatings is determined by its resorption time which has a specific time frame. The resorption or corrosion rate is usually not constant and a special study is required in order to predict the rate of change for long periods of time. Thicknesses can be used as a parameter to specify a time frame for the effects of a coating if the resorption rate of the coatings can be modeled or predicted. Since Mg-based materials typically dissolve or corrode in aqueous media at reasonably high rates, this issue can be addressed through the use of coating thickness as a factor for resorption time.

1.2 Objectives

The objective of this study is to develop biocompatible, functional magnesium oxide (MgO) coatings that:

i. serve as galvanic separators between metallic substrates and metallic coatings,
ii. control the rate of corrosion of Mg-based implants,
iii. have controlled resorption times based on coating thickness,
iv. promote osseointegration and
v. are predictable in corrosive environments.

CHAPTER 2

LITERATURE REVIEW

2.1 Biomaterials

2.1.1 Introduction

Diseased tissues have been treated with biomaterials dating back more than 2000 years, with some early examples being wooden teeth and glass eyes. Since there was a poor understanding of biocompatibility prior to the 1960s, biomaterials such as these had low success rates. As World War II came to an end, materials that had been initially developed for military purposes became available for common use. Ceramics, inert, durable metals and polymers such as Poly(methylmethacrylate) (PMMA), were being used for clinical applications and were also being used by surgeons. The absence of cytotoxicity was used to determine the biocompatibility of these industrial materials since they were not redesigned specifically for biomedical purposes. These advances sparked an entirely new field of research which was introduced in the 1960s and focused on new biomaterials with enhanced biological performance. The focus of biomaterials research was progressively shifting from engineering and materials science toward a more integrated methodology, which involved material scientists, biologists and surgeons, and as a result of this, a paradigm shift occurred around the 1990s.

Research efforts became directed at replacing and improving biological functions by combining biologically active molecules, cells and carrier materials called scaffolds. These developed into the three key fundamentals of tissue engineering. Another key step

in the advancement of biomaterials was the coming together of tissue engineering and stem cell research during the early 2000s which resulted in the more extensive field of regenerative medicine. The central point of regenerative medicine lies in human cells which compares the prominent role of artificial biomaterials throughout the ages of tissue engineering and biomaterials. Two differing approaches in regenerative medicine were determined by Shastri: (i) tissue architecture generated externally and (ii) specific wound healing induced by minimal intervention through the design of materials (Shastri, 2006). Regenerative medicine produces a new generation of materials that are instructive which coordinate local cellular practices by implementing signaling functions that result from biological processes (Leeuwenburgh *et al.*, 2008).

2.1.2 Polymers

Polymers are considered to be the most extensively used biomaterials. Polymers are long chain, organic molecules that are versatile in their properties and composition. Some common natural polymers include heparin, DNA, collagen and hyaluronic acid. Some benefits of using polymers in biomedical applications are versatility, reasonably low cost and ease of manufacturing. Polymers are composed of covalently bound repeating units called monomers. These monomers are linked together with a common backbone and they form a large molecular chain. Different networks of polymer chains can be cross linked together, which results in interconnections between the molecules. Different types of physical or chemical bonding can be comprised from these crosslinks. Polymers can be considered crystalline if these interconnected networks of molecular chains have a long range order, or amorphous in the absence of such an order.

Over the past 35 years, biodegradable polymers have evolved. Once these materials are implanted they are gradually replaced by tissues that are regenerated in vivo and break down into a safe product that is later removed and/or metabolized by the body. Common examples of degradable synthetic polymers are Poly(lactide-coglycolide) (PLGA), polyanhydrides and polycaprolactone, while chitin, starch, collagen and glycosaminoglycans are polymers that degrade naturally. Several methods can influence the rate of material degradation of polymers such as varying chain length (molecular weight), crystallinity degree, glass transition temperature and local conditions.

2.1.3 Ceramics

Ceramics are nonmetallic, inorganic materials that have biological inertness and superior strength in compression that make them advantageous in medical applications. Metallic oxides, carbides and sulfides are examples of ceramics. Ceramics are generally known for their hardness and are limited by their poor mechanical properties and brittleness. Other beneficial properties of ceramics are low electrical conductivity, high melting point, and low thermal conductivity. Many useful biocomposites and bioceramics have been developed due to advancements in this field, and they are normally classified into one of these categories: bioreactive, completely reabsorbable and bioinert.

Bioceramics that are resorbable degrade over a period of time and endogenous tissues replace them with functional, normal bone in orthopedic applications. Their ability to allow for osteoblast integration or osteoconductive capability leads to osteoid creation, which is a key property. Materials such as hydroxyapatite, calcium phosphate and calcium sulfate dehydrate (Plaster of Paris) are considered reabsorbable bioceramics.

During the resorption process the mechanical properties of these materials are reduced greatly, which results in a considerably different load-bearing capacity over the progression of integration. The key characteristic of bioreactive bioceramics is the capability of the material to bond chemically and interact with normal tissue at its interface.

2.1.4 Composites

Composite materials are made from two or more fundamental materials with different physical, chemical or mechanical properties. Composites are typically composed of at least one discontinuous phase embedded in a continuous phase called the matrix. This is particularly different from mixtures that are homogenous, like metallic alloys, because each of the materials maintains its own unique properties. The overall performance of the composite is heavily dependent on the transfer of forces at the interface of the materials. Other considerations that are important in the performance of composites are orientation, shape and volume fractions. Fibrous and particulate composites are typically the two different types of composite biomaterials.

Particulate composites consist of small particulates in a continuous matrix. These materials are usually isotropic with increased toughness in every direction. With this increased toughness, stiffness and flexibility is sacrificed. Dental composites made with ceramic matrices, silica particles and rubber catheters reinforced with silica particles are examples of these materials. Particulate composites where the inclusion phase is air are a special type of composite called porous materials. These porous materials are used in both hard- and soft-tissue applications. Porous composites have the ability to promote

tissue ingrowth. Fibers that are immobilized in a matrix are called fibrous composites. An example of a fibrous composite is a carbon-reinforced polyethylene for the replacement of joints. Laminates, which are composed of multiple layers of stacked fiber composite laminae, are a special class of fibrous composites.

2.1.5 Metals

Metals are inorganic materials that have bonding characteristics and unique atomic arrangements that lead to enhanced thermal, electrical and mechanical properties. Their loadbearing-properties, mechanical strength and conductivity make them perfect for multiple medical applications including dental implants, fixation devices, prostheses for hard tissue replacement, and active devices such as electrodes, stents and guide wires. A unique consideration for the biocompatibility of metals is that corrosion may occur in physiological situations. Corrosion is a chemical reaction that leads to the progressive weakening of the deteriorating material and releases products into the contiguous surroundings which could possibly lead to adverse effects. Metals that are noble, such as platinum, silver and gold are inert and are not subject to corrosion reactions. Metals that produce thin oxides have the ability to form an inert, adherent layer that prevents further reactivity between the biological system and the metal. Metals that usually form strong oxide layers include chromium and titanium. Clinically, corrosion may manifest as local swelling or pain without evidence of discoloration, infection or flaking of the implant which is detected visually during surgery.

A majority of metals are not useful biomaterials because of corrosion and biocompatibility concerns. Even though metals that are noble show exceptional corrosion

resistance and excellent biocompatibility, the load-bearing properties are not ideal. Consequently, a few of these materials are represented in biomaterial applications. Other pure metals that have found use in biomaterial applications are magnesium (Mg), the platinum group and tantalum. Mg has been found to be a very useful biomaterial in the areas of cardiovascular and orthopedic devices. Though Mg has low corrosion resistance, its mechanical properties are advantageous. Neither the platinum group of metals nor tantalum has good mechanical properties, though they do exhibit high corrosion resistance.

Two or more metals that are homogenously mixed form what is called an alloy. The first metal alloy that was specifically developed as a biomaterial was vanadium steel. Vanadium steel is no longer in use because it was found to be very susceptible to corrosion. The most common alloys that are currently in use are titanium (Ti)-containing, cobalt-chromium, stainless steel and shape memory alloys. Stainless steel alloys are a mixture of iron, nickel, chromium, carbon, manganese and other trace elements. Cobalt-chromium alloys contain chromium and cobalt as well as other minor elements. Cobalt-chromium alloys exhibit a performance similar to stainless steel with enhanced corrosion resistance and slightly higher or comparable mechanical properties; however, metal ions have been observed slightly leaching into the tissues.

Titanium and Ti-containing alloys are in extensive use due to their low density and good mechanical properties, which give these alloys a high strength-to-weight ratio as well as a favorable biocompatibility profile. The good biocompatibility profile is due to an adherent oxide layer forming. Ti-containing alloys are ideal due to their distinctive

properties in applications which require high load-bearing without adding too much weight to the joint or limb. A unique nickel-titanium alloy known as nitinol possesses all the properties of Ti but also has shape memory, fatigue resistance, superelasticity, force hysteresis and kink resistance. One of nitinol's most significant characteristics is shape memory which allows the material to return to a thermally predetermined shape after it has been deformed by raising the temperature beyond its point of transition, which is typically at body temperature. The material can also be deformed 20 times more than stainless steel due to its superelasticity. Nitinol is also compatible with MRI since it is nonparamagnetic (Binyamin, Shafi, & Mery, 2006).

2.2 Magnesium as a Biodegradable Implant

2.2.1 Introduction

Elemental Mg was discovered by Sir Humphrey Davy in 1808 and shortly after this the biodegradable Mg implant came into existence. In 1833, Michael Faraday, Davy's assistant, produced Mg metal through the electrolysis of fused anhydrous $MgCl_2$ and in 1852 a small laboratory cell was created by Robert Bunsen for the electrolysis of fused $MgCl_2$. At this time, in America and Europe, Mg was produced in small quantities for use in pyrotechnics and for igniting wires or bands for flash lights in photography. These preliminary uses for Mg were displayed in London in 1862 at the world exhibition. It is presumed that some of those Mg wires were used as ligatures to stop the bleeding of human patients in 1878 by physician Edward C. Huse. These ligatures effectively stopped bleeding three times: twice in the operation of a varicocele and once in a radial artery. At

this time Huse had already perceived that Mg corroded slower *in vivo* and that the time for complete degradation depended on the size of the Mg wire used. As a result of this, Huse wrote very strongly about the degradation properties of Mg (Witte, 2010).

Mg and its alloys are used extensively in the aerospace and transport industries, primarily due to their high specific strength to weight ratios. Some of the key disadvantages of Mg and its alloys in these applications are their low elastic modulus, low corrosion resistance, limited creep resistance and limited strength at higher temperatures. In the human body, Mg is a vital element and is generally found in bone tissue since its presence is beneficial to bone growth and strength. Mg ions are the fourth most abundant cations in the human body and normal adults require 300-400 mg daily. Several metabolic enzymes require Mg as a co-factor and it also stabilizes the structure of RNA and DNA. A deficiency in Mg can cause increased occurrences in cancer, heart disease, susceptibility to oxidative stress and cell membrane dysfunction. A surplus of Mg can lead to hypotension, muscular paralysis, cardiac arrest and respiratory distress however, this surplus is very unlikely due to efficient filtration by the kidneys. It has been considered safe to produce Mg for use as implantable materials since the human body has a high daily requirement of Mg. Mg and its alloys have been used in orthopedic implants because their properties are comparable to human bone. The density of Mg is similar to natural bone (1.8-2.1 g/cm^3) and it has been reported that Mg supports in the initial formation of bone cells. The major limitation in the use of Mg-based implants is their low corrosion resistance. Some techniques that can be used to increase the corrosion resistance of Mg are alloying, coating and heat treatment. In order to give the body time

to regulate the OH^- and gaseous H_2 that might be generated during the degradation process, it is necessary to slow the degradation rate of Mg and its alloys (Mantovani, Purnama, Hermawan, & Couet, 2010).

Commercial implants containing Mg and its alloys are still not available though they have been studied as implants for almost two centuries. The benefits and advantages of biodegradable Mg and its alloys have gained great interest from researchers and clinicians within the last decade, which has led to further investigations into biomedical applications and exploring the limitations of their clinical use. Special care should be taken by clinicians and researchers in considering that Mg is a lightweight metal that requires a distinctive knowledge. Experience-based design and careful professional handling is needed in order for a successful biomaterial to be created (Witte, 2010).

2.2.2 Advantages of Mg-based Implants over Permanent Implants

Metallic materials play a significant role as biomaterials in assisting with the replacement or repair of bone tissue that has become damaged or diseased. In comparison to ceramics and polymers, metals are more suitable as implant materials for load-bearing applications due to their high fracture toughness and mechanical strength. The most commonly used non-biodegradable, metallic biomaterials are made of medical-grade metals such as Ti and its alloys, 316L stainless steel and cobalt-chromium based alloys. A major drawback of these current biomaterials is the potential release of particles and/or metallic ions that are toxic. This can lead to local inflammation which causes tissue loss and signifies a lack of biocompatibility. If this were to happen, a second surgery would need to be performed for implant removal.

With repeated surgeries, morbidity rates of the patients is increased, which leads to an increase in health care costs and longer hospitalization. These complications would be drastically reduced with the use of Mg-based metallic, biodegradable implants. Another disadvantage of currently used metallic materials is that the elastic moduli do not match well with natural bone tissue (Table 2.1).

Table 2.1. Mechanical and physical properties of implant materials in comparison to natural bone (Pietak, Staiger, Huadmai, & Dias, 2006)

Properties	Natural bone	Mg	Ti alloy	Co–Cr alloy	Stainless steel	Synthetic hydroxyapatite
Density (g/cm^3)	1.8–2.1	1.74–2.0	4.4–4.5	8.3–9.2	7.9–8.1	3.1
Elastic modulus (GPa)	3–20	41–45	110–117	230	189–205	73–117
Compressive yield strength (MPa)	130–180	65–100	758–1117	450–1000	170–310	600
Fracture toughness ($MPam^{1/2}$)	3–6	15–40	55–115	N/A	50–200	0.7

The dissimilar mechanical and physical properties of current implants to natural bones could potentially lead to stress shielding effects which results in decreased implant stability from remodeling, and reduced stimulation of new bone growth. Current metallic biomaterials remain permanent fixtures, typically neutral *in vivo* and the screws, plates and pins used to secure severe fractures need be removed through a subsequent surgical procedure after the tissue has healed satisfactorily (Pietak *et al.*, 2006). Figure 2.1 shows

bone-implant osseointegration and interface strength of a biodegradable Mg alloy implanted into a rat to show that the Mg alloy demonstrated properties at least equal to typical titanium rod implants.

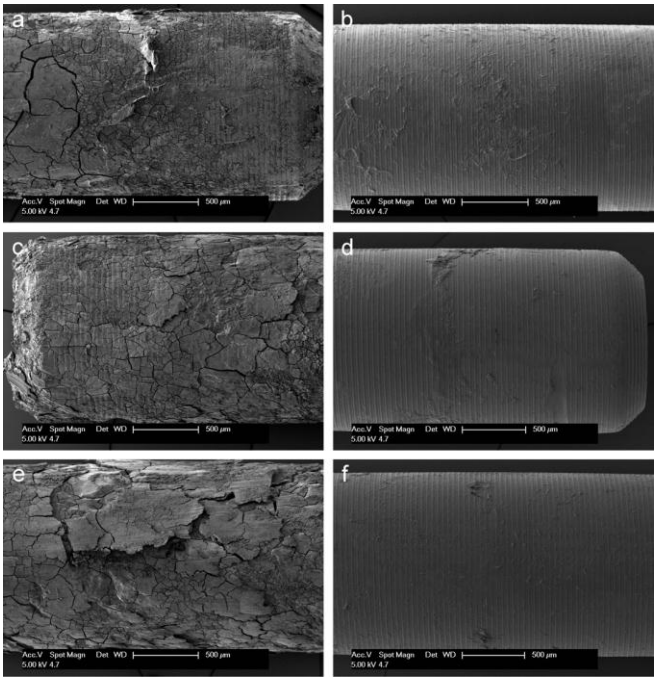

Figure 2.1. SEM images of implants that were tested. Biodegradable Mg alloy rods (a,c and e) and Ti6Al7Nb controls (b, d and f), 12 (c and d) and 24 (e and f) weeks after implantation. (Lindtner *et al.*, 2011)

This study showed that the osseointegration and bone-implant interface strength of the biodegradable Mg alloy in comparison to the standard Ti alloy control in the rat model was significantly greater. It was also shown that the *in vivo* degradation of the Mg implant does not affect the blood composition, nor does it encourage a systematic inflammatory reaction. The µCT showed that there was an improved reaction to the Mg alloy, which was shown by a considerable increase in bone implant contact and higher trabecular bone volume per total tissue volume. These results showed that the Mg alloy

that was tested reaches a higher osseointegration and stability than the Ti implants that are currently used after having been implanted in rats transcortically for 4, 12 and 24 weeks. Contrary to commonly used steel or titanium implants, the need for a second intervention to remove an implant would be eliminated through the use of biodegradable Mg implants. This would reduce the stress shielding effects due to its elastic modulus being close to the elastic modulus of natural bone. Biodegradable Mg implants have excellent mechanical properties, which make them more suitable for load-bearing applications (Lindtner *et al.*, 2011).

2.2.3 Corrosion of Magnesium

Magnesium and its alloys are generally known to degrade in aqueous atmospheres through an electrochemical reaction which creates hydrogen gas and magnesium hydroxide $Mg(OH)_2$. As a result of this, Mg corrosion is relatively unaffected by a variety of oxygen concentrations in aqueous solutions which are seen around implants in various anatomical situations. In aqueous environments, the overall corrosion reaction is:

$$Mg_{(s)} + 2H_2O_{(aq)} \leftrightarrow Mg(OH)_{2\,(s)} + H_{2\,(g)}$$

$Mg(OH)_2$ accrues as a corrosion protective layer in water on the underlying Mg matrix, but when the chloride concentration rises above 30 mmol/L in the corrosive environment, $Mg(OH)_{2\ (s)}$ begins converting into highly soluble magnesium chloride. Thus, severe pitting is observed *in vivo* on Mg alloys where the chloride content is about 150 mmol/L in the body fluid. Elements and cathodic sites with low hydrogen overpotential enable hydrogen evolution in Mg and its alloys which causes extensive galvanic corrosion rates

and possible local gas cavities *in vivo*. The alloy composition and environmental conditions determine the corrosion morphology of Mg and its alloys (Witte *et al*., 2008).

Galvanic corrosion is an electrochemical process in which two metals are in electrical contact and one metal corrodes preferentially over another. Metals and alloys that are dissimilar have different electrode potentials and when these metals come in contact with one another in an electrolyte, a galvanic couple is formed. This electrolyte offers a means for ions to migrate whereby metallic ions can move from the anode to the cathode. As a result, the anodic metal corrodes quicker than it normally would and the corrosion of the cathodic material slows down and in some instances stops. A conducting path is formed between the metals through the presence of the electrolyte and causes corrosion to occur (Wikipedia, 2011). Table 2.2 gives the corrosion potential, E_{corr}, of some common engineering alloys and shows that Mg is more active than all the engineering alloys. As a result of this, Mg is the anode in galvanic couples.

Table 2.2. Common engineering alloys and their typical corrosion potential values (Atrens, Liu, & Abidin, 2011)

Metal	E_{corr}, V_{SCE}
Mg	-1.65
Zn	-1.02
Al-7075	-0.88
Al-1xxx	-0.73
Fe	-0.50
Cu	-0.12
Ni	+0.01

Galvanic effects are always an issue for Mg due to its active nature (Atrens *et al.*, 2011). Pitting or the formation of local corrosion cells on the surface is caused by electrolytic contact with another metal. In order for a metal coating to battle this issue it must be pore free. If the metal coating is not pore free, there will be an increase in the corrosion rate of the material. In outdoor uses for Cu-Ni-Cr alloys a minimum pore-free coating thickness of 50 µm is suggested (Luan, & Gray, 2002). Figure 2.2(a) shows macro-galvanic corrosion when coupled with a material that is a less active metal and Figure 2.2(b) shows micro-galvanic corrosion.

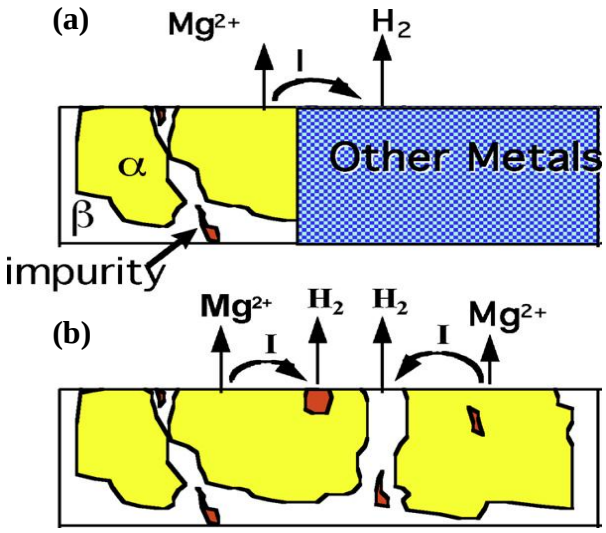

Figure 2.2. (a) Macro-galvanic corrosion, (b) Micro-galvanic corrosion (Atrens *et al.*, 2011)

Figure 2.2(a) is a schematic representation of Mg forming a galvanic couple with a material that is dissimilar. The schematic shows Mg ions migrating to the other metal and Mg is corroding as a result of this. While Mg is corroding the other metal's corrosion is slowed. Figure 2.2 also shows the release of hydrogen gas (H_2) which is a result of Mg

corrosion reactions. Figure 2.2(b) shows Mg galvanic corrosion with no dissimilar metal present. Micro-galvanic corrosion is similar to macro-galvanic corrosion due to Mg being the anode in both cases. However, the cathode in micro-galvanic corrosion is caused by secondary phases within the Mg (Atrens *et al.*, 2011).

2.2.4 Corrosion Resistance

Poor corrosion resistance of Mg alloys is a result of (1) the high inherent dissolution propensity of Mg, which is slightly repressed by the film of corrosion products, and (2) local micro-galvanic acceleration of corrosion due to the existence of second phases that act as local cathodes. Mg alloy corrosion typically begins on various parts of the exposed surface and then extends over the entire surface. As immersion time increases, so does the corrosion rate. In the early stages in chloride containing solutions, the corrosion rate is observed as being low. This data is partly controlled by the breaking down of film that is on the surface at the start of immersion.

Any biomaterial in the body, whether degradable or inert, induces reactions in the body from surrounding tissues that are identified as “host responses”. In order to assess the biocompatibility of a biomaterial, the host responses are used as parameters. Biocompatible biomaterials should show a miniscule amount of toxicity and inflammatory responses, both systemically and locally. Products of degradation that occur from corrosion processes of biodegradable metallic materials have the potential, once they interact with biological surroundings, to produce reactions which, to the body, is possibly unknown, new and perhaps unexpected. This is why it is absolutely necessary to conduct biocompatibility tests to explore the possible toxic potential and inflammatory

reaction of the neighboring tissues based on the possibility of the elements released on contact between the cells and the metals. The trial is to evaluate the tolerance of neighboring tissues in the presence of degradation products (Atrens *et al.*, 2011).

2.2.4.1 Alloying

The mechanical properties, corrosion resistance and manufacturability of Mg-based materials can be improved with an appropriate alloy composition (Pietak *et al.*, 2006). The current Mg alloys that are being explored for implant applications are commercially available alloys which have been developed for uses in the transportation industry. The system used to categorize Mg alloys follows the nomenclature of the American Society for Testing and Materials (ASTM). There are three major groups that Mg alloys can be divided into: pure Mg with trace elements, alloys that contain aluminum (Al) and Mg alloys that have no Al. Mg alloys that usually contain Al are AZ91, AZ31, AE21, LAE442 and calcium (Ca) modified AZ alloys. Over the decades AZ31 and AZ91 have found use in a variety of technical applications. Other elements that can be found alongside the elements Al and zinc (Zn) are small amounts of manganese (Mn), rare earth elements (RE) and lithium.

The Mg alloys that are Al-free are WZ, MZ, WE and Mg-Ca alloys. The WE43 Mg alloy has been designed to remain stable at high temperatures and to increase creep resistance. This alloy contains RE, zirconium (Zr) and yttrium (Y). Though these Mg alloys are heavily used, none of these alloys were specifically made for use as a biodegradable implant material. These alloying elements that are used affect the Mg alloy's physical and mechanical properties. Most of these alloying elements can react

with Mg or amongst each other to form intermetallic phases. The alloy is strengthened by these phases through precipitation strengthening. If these alloying elements stay in a solid solution, they can also be used for solid solution strengthening. Even though the strength of these alloys is improved by both precipitation strengthening and solid strengthening, the alloy's ductility deteriorates. However, the grains are refined to some extent by these alloying elements by a strengthening mechanism known as Hall-Petch strengthening or grain boundary strengthening. This type of strengthening improves the ductility and strength (Witte *et al.*, 2008).

2.2.4.2 Coatings

In orthopedic uses, the objective of Mg protective coatings must be to improve the bioactivity/biocompatibility of the implant and it must also be non-toxic (Pietak *et al.*, 2006). One of the most effective ways to prevent Mg corrosion or to slow the corrosion process is through coatings. Coatings are useful because they protect the substrate by providing a protection barrier between the metal and its surroundings and/or through the presence of chemicals that have corrosion inhibitors in them. Coatings that provide satisfactory corrosion protection must be pore free, uniform, adhere well and be self-healing in applications where physical damage to the coating may occur (Luan *et al.*, 2002).

An electrolytic procedure for creating a stable, thick film on alloys and metals is known as anodizing. The process includes the use of either a DC or AC current with the films forming a thin barrier layer at the interface of the metal and the coating. A cellular structure layer is then applied with each cell containing a pore size that is determined by

its concentration and the type of electrolyte, current density, temperature and the voltage applied. The quality of sealing of the anodized film is determined by their size and density. In order to attain a corrosion-resistant film, it is essential to seal the anodized film. This is done by sealing off the porous oxide film through precipitation of the hydrated base metal inside the pores. Hardness and wear resistance of the anodized films can be enhanced by decreasing the electrolyte temperature and increasing the current density.

A major challenge in creating corrosion resistant, adherent, anodic coatings on Mg is the result of phase separation in the alloy due to electrochemical inhomogeneity. Uneven deposition could also be an outcome due to flaws, inclusion and porosity from mechanical pretreatment. Uniform throwing power can also be difficult to achieve due to areas of shapes with narrow cavities, deep recesses or sharp corners. Defects in the coatings can actually intensify corrosion. Another disadvantage to this method is the base metal's fatigue strength can be affected during the treatment by localized heating at the surface particularly in thicker films.

The deposition of a solid on a surface that is heated through a chemical reaction from the gas phase is called chemical vapor deposition (CVD). Some of the benefits of this method are grain size and orientation control, good adhesion, processing at atmospheric pressure and attaining near-theoretical density. Since high deposition rates can be accomplished through CVD, thick coatings are capable of being created. This process is restricted to substrates that are thermally steady at or above 600ºC, though efforts are underway to combat this issue. Another drawback to the process is that the

chemical precursors are toxic in nature which makes it necessary to use a closed system. Waste disposal costs are also introduced since toxic solid byproducts can be created. This method can also be costly due to the need for depositions at high temperatures and low efficiency in the process.

Physical vapor deposition (PVD) is a deposition process that involves molecules or atoms deposited from the vapor phase onto a substrate. This process includes pulsed-laser deposition, ion plating, sputter deposition, vacuum deposition and diffusion coatings. The deposition of corrosion and wear protection coatings and creating bulk Mg alloys with corrosion resistant properties that are distinctive are the two key duties of PVD in Mg surface finishing. In coating Mg substrates, there are a few challenges that must be overcome. The temperature during deposition must stay below the stability temperature for Mg (180ºC) and, despite this low temperature, good adhesion must occur. The coating must also be resistant to corrosion. (Luan *et al.*, 2002).

2.2.5 Magnesium Oxide

Magnesium alloys are increasingly being used in the automotive industry as structural materials to reduce the weight of vehicles. Some applications of Mg alloys in the automotive industry are valve/cam covers, instrument panel beams, manual transmission cases, steering components and various brackets and housings. In order to combat corrosion resistance, a number of coating techniques such as Plasma Electrolytic Oxidation (PEO) have been investigated. Nie *et al.* used PEO to form oxide coatings on the surface of Mg in order to improve corrosion and wear resistance. The coatings were designed to protect the Mg engine block from galvanic corrosion occurring near the

cylinder gasket with various coating thicknesses being investigated. During the PEO process, the stainless steel plate acted as the cathode and the coupons acted as the anode as seen in Figure 2.3.

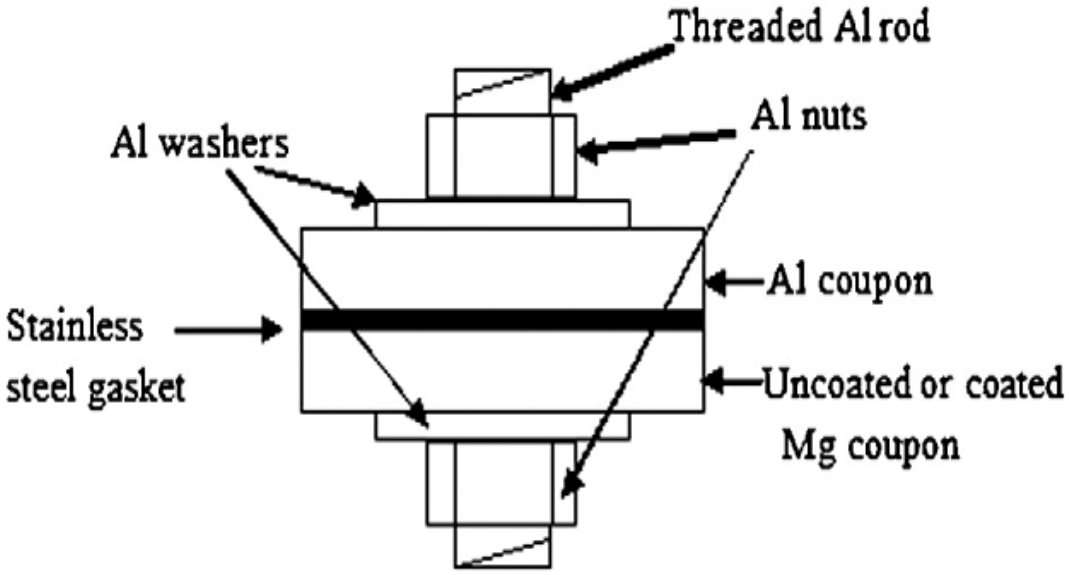

Figure 2.3. Schematic drawing of galvanic corrosion test sample (Nie, Zhang, & Northwood, 2009)

SEM was used to measure coating thickness and to observe the coating surface morphology. The PEO coatings on pure Mg showed improved erosion and corrosion properties in comparison to the substrate. Polarization resistance and anti-galvanic corrosion resistance of the coated samples increased as the coating thickness increased. Acceptable protection of Mg against galvanic corrosion was seen with a coating thickness of 5 μm (Nie *et al.*, 2009).

Bandyopadhyay *et al*. investigated the influence of MgO, ZnO and SiO_2 dopants on the biological, physical and mechanical properties of tricalcium phosphate (TCP)

resorbable ceramics (Bandyopadhyay, Bernard, Xue, & Bose, 2006). Special emphasis was put on the study of cell-materials interactions and *in vitro* strength degradation with respect to time. This study showed that TCP-MgO-ZnO showed exceptional biocompatibility with the osteoblastic precursor cell line 1 (OPC1) cells. These results suggest that this sample, doped with MgO and ZnO, promotes better cell spreading behavior and attachment than TCP alone.

In the packaging industry, incorporating antimicrobial agents directly into packaging films that come into contact with food materials, drugs and cosmetics is a commercially attractive idea. Manorama *et al*. found that, due to the formation of superoxides at the surface, MgO particles (nano-MgO) have been reported to possess antibacterial activity. Nano-MgO shows high activity against spores, viruses and bacteria because of its large surface area, positively-charged particles and abundance of crystal defects, which can result in strong interactions with negatively-charged spores and bacteria. In this study, coagulated clumps appeared due to the interactions of bacteria with nano-MgO because of electrostatic aggregation of particles, which penetrate the bacterial cells. As particle size decreased, the activity increased.

Fourier transform infrared spectroscopy was performed to observe the toxicity in order to analyze the bacterial membrane for chemical reactions that may have resulted from interaction with the nano-MgO particles. Chemical changes occurred in the proteins in the cell wall of the bacteria due to the considerable increase in intensity of the C-O stretching vibration. It was also reported that MgO is readily hydrated which leads to a layer of $Mg(OH)_2$ forming on the surface. From this layer a super oxide layer is formed

which causes membrane malfunction and bacteria cell death. It was concluded that nano-MgO may be superior to TiO_2 since TiO_2 is only photoactive and useless against B. *subtilis* spores (Manorama, Basakand, & Singh, 2012).

Ahmed *et al*. found that adding MgO nanoparticles to Poly(methyl methacrylate) PMMA has been shown to drastically reduce the temperature during the solidification process of PMMA, which reduces the damaging effects of the exothermic reaction on surrounding bone. As a result of this the degree of osseointegration improved. Surfaces that have higher nanoroughness increase osteoblast functions. One explanation for this is that the protein size that acts as a mediator for osteoblast adhesion is in the nanometer range. A surface that has nanotopography influences the opportunity for protein's cell adhesion to a greater degree than standard surfaces that are nanosmooth. Osteoblast adhesion is increased because of electron delocalization for nanoscale materials.

More surface area is available for nanophase materials and this leads to greater delocalization of electrons. This was illustrated through the use of MgO which has a less acidic OH^- group on the surface due to a high proportion of edge sites for nanophase MgO, which causes the delocalization of electrons. More electronegative surfaces are created in high electron delocalization nanophase materials compared to conventional materials and this increases electrostatic attractions between proteins and surfaces which cause a drastic change in the way the proteins interact with the surfaces. Protein adsorption rate increased on nanophase surfaces and this is a result of the change in electrostatic attractions (Ahmed, & Seifalian, n.d.).

2.3 Magnetron Sputtering

2.3.1 Introduction

In the industry, magnetron sputtering is one of the approaches regularly used to deposit high quality thin films (Welzel, Dunger, Liebig, & Richter, 2011). In many instances, magnetron sputtering can offer the same functionality as films that are much thicker that are produced by other PVD surface coating methods. Another major reason why magnetron sputtering is commonly used is the possibility to grow film with high deposition rates on substrates that have large areas (Kelly, & Arnell, 2000). Some of the factors that affect the performance of the coatings are chemical and phase composition, microstructure and adhesion to the substrate. The interface between the substrate and the coating determines adhesion (Musil, & Vlcek, 1999). A critical parameter in all PVD processes is ion bombardment of the critical film which has a strong influence on the properties and structures of the growing film.

In basic sputtering processes, a cathode or target plate is bombarded in a glow discharge plasma by energetic ions that are created in front of the target. During the bombardment process the removal or sputtering of target atoms takes place and these atoms condense on a substrate to create a thin film. As a result of the ion bombardment secondary electrons are also emitted from the surface of the target. These secondary electrons play an important role in sustaining the plasma. In magnetron sputtering systems the magnetrons use a magnetic field that is arranged parallel to the target surface. This allows the magnetron to restrain the secondary electrons to the target area. The magnets are arranged where one pole is situated at the target's central axis and the second

pole is formed by a ring of magnets that extend around the outer edge of the target. The probability of an ionizing electron-atom collision happening is improved by trapping the electrons in this way. A dense plasma in the target region is the result of the increased ionization efficiency of the magnetron. As a result, this leads to a better ion bombardment of the target which gives higher sputtering rates and higher deposition rates (Kelly, & Arnell, 2000).

2.3.2 Reactive Sputtering

Sputtering elemental targets in the presence of chemically reactive gases (RG) that mass react with both the surface of the target and the material ejected from the target is defined as reactive sputtering. Reactive sputtering has become a very popular method for the deposition of a wide variety of alloy and compound thin films, which include nitrides, oxides, fluorides, carbides or arsenides (Safi, 2000). Depending on the amount of RG used in the film deposition, the reactive sputtering process can be divided into three modes: (a) metallic, (b) transition and (c) reactive. A decrease in the deposition rate is seen when the film is sputtered in the reactive mode due to the reaction of the RG with the surface of the target that is being sputtered and its conversion to a compound. The decrease in deposition rates is strongly dependent on the target material and the kind of reactive gas (Musil, Baroch, Vlcek, Nam, & Han, 2005).

2.3.3 Pulsed Sputtering

In recent years, Pulsed Direct Current (PDC) magnetron sputtering has been used in a wide variety of research and industrial applications because of its effective ability to suppress arcs, extensive range of process parameters adjustment and high plasma density

at the substrate. PDC is also used because of its stable and high deposition rate of semiconductors and insulators in comparison to continuous DC and radio frequency (RF) sputtering processes (Karthikeyan, Hill, Cowpe, & Pilkington, 2010). Though high quality films can be produced through direct RF sputtering of an oxide target, RF sputtered films have deposition rates that are very low. When the magnetron is pulsed in the medium frequency range of 10-200 kHz during the deposition of insulating films, the formation of arcs is considerably reduced and consequently, the number of defects in the resulting film is reduced. This allows the deposition rates achieved through PDC to almost reach those obtained during the deposition of pure metallic films (Kelly, & Arnell, 2000). Generally, PDC films are significantly harder and denser than those achieved from a DC process (Brauer, Szyszka, Vergohl, & Bandorf, 2010).

An oxide film may be formed during DC reactive sputtering of an oxide from an elemental target. Positive ions that are accelerated in the plasma collect on the surface and charge this insulating layer. If infinite electric field strength could be sustained by this insulating layer, then this layer would eventually be charged to the applied power supply voltage. As a consequence, no potential would be left to accelerate electrons and ions in the plasma and this would cause the sputtering process to stop. However, the insulating film can tolerate electrical field strengths up to 1 – 10 MV/cm before an electrical breakdown in the layer occurs. During this breakdown or micro-arcing period, small particles can be ejected from the arcing tracks, which may cause these micro particles to reach the substrate and become embedded in the growing film. Arcing at the

target, as seen in Figure 2.4, can be eliminated by creating certain conditions through a PDC power supply.

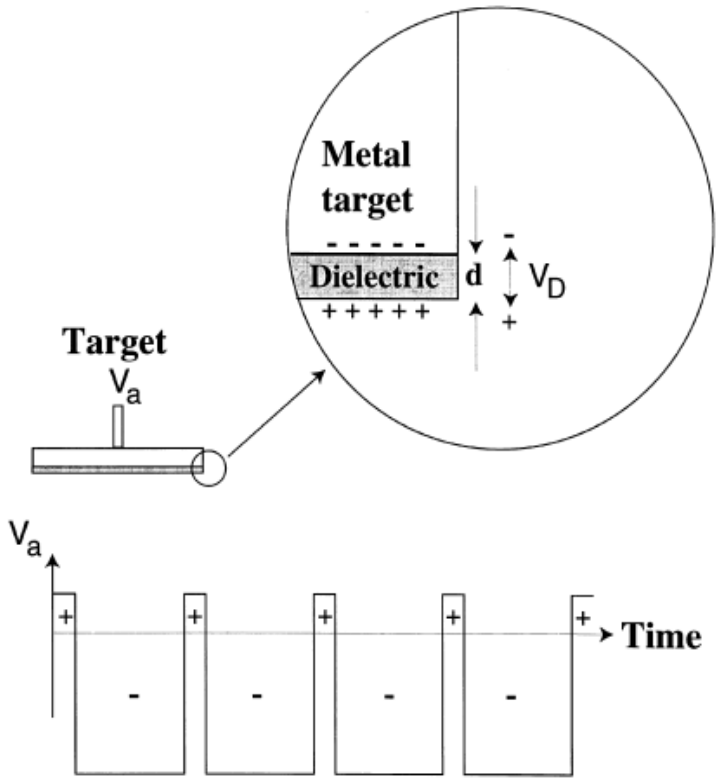

Figure 2.4. Schematic of bipolar target voltage in PDC process (Berg, Jonsson, Nyberg, Katardjiev, 2000)

The voltage build up on the insulating layer can be regulated by interrupting the negative voltage and applying a short positive pulse to the target. Electrons are attracted to the target through this positive pulse and this flux of negative particles will partially or fully discharge the insulating layer (Berg *et al.*, 2000). Figure 2.5 shows a schematic representation of an asymmetric bipolar target voltage which represents a constant voltage mode of -450 V operating at 100 kHz.

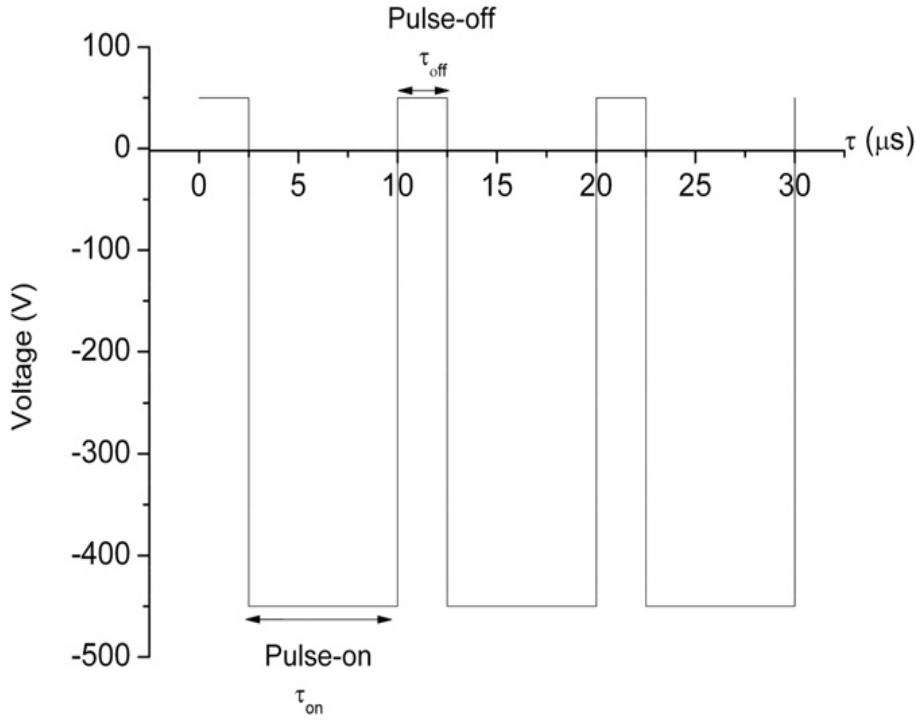

Figure 2.5. Schematic representation of 100 kHz pulsed DC signal with a pulse-off time τ_{off} of 0.25 µs and pulse-on time τ_{on} of 0.75 µs (Karthikeyan *et al.*, 2010)

The duty cycle of the signal is 75% which means the negative signal will last for 7.5 µs with one complete cycle duration of 10 µs. This 7.5 µs is referred to as the pulse-on time (τ_{on}) period. The remaining 2.5 µs, known as the pulse-off time (τ_{off}), is ideally at zero or a few positive volts and this period alleviates charging problems connected with DC reactive sputtering of dielectric materials by discharging the regions that are charged on the target during the reverse voltage stage (Karthikeyan *et al.*, 2010). Figure 2.6 depicts SEM micrographs of aluminum oxide deposited using both DC and PDC reactive sputtering. Figure 2.6a is an SEM micrograph of the fracture section of a DC reactive sputter deposited aluminum oxide coating.

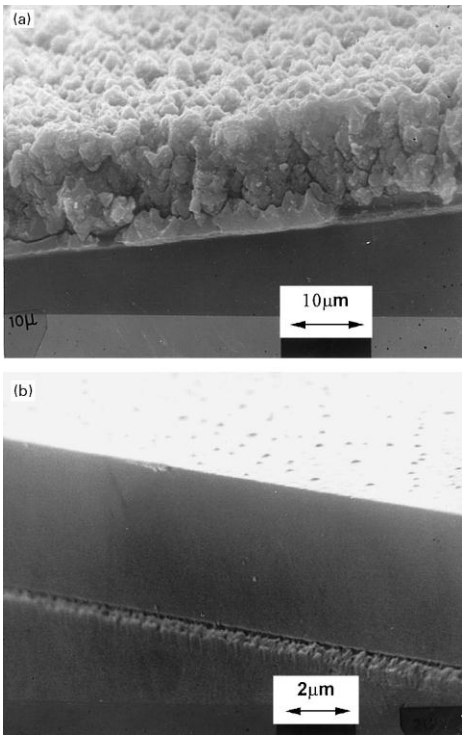

Figure 2.6. SEM micrographs of aluminum oxide fracture sections deposited by (a) DC reactive sputtering, and (b) pulsed DC reactive sputtering (Kelly, & Arnell, 2000)

The micrograph shows that the deposition process was very unsteady with arcing occurring at the target. The coating has a porous, granular structure with a composition that is sub-stoichiometric. In contrast, Figure 2.6b is an SEM micrograph of the fracture section of a PDC reactive sputter deposited aluminum oxide coating. During the deposition arc events were inhibited and the process was very steady. Therefore, the stoichiometric composition of the coating was Al_2O_3 and was very dense with no apparent structural defects or features (Kelly, & Arnell, 2000).

R.D. Arnell *et al.* used pulsed power in the range of 100-350 kHz and investigated the coating properties and the resulting plasma parameters. Measurements were made in both non-reactive and reactive environments, alongside film deposition. Ti films that

were deposited at low frequency <50 kHz and at frequencies >300 kHz displayed a higher surface roughness. In the range of 50-300 kHz, the surface roughness remained stable. This can be seen in Figure 2.7, which assesses the appearance of the surface of films grown at 100 and 350 kHz.

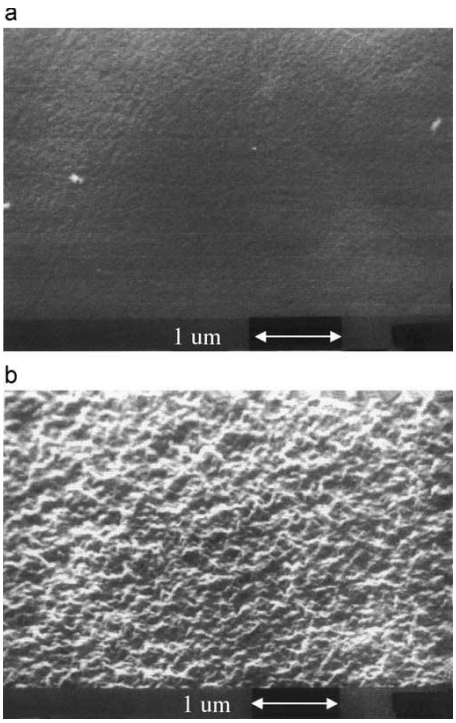

Figure 2.7. SEM micrographs of the top surface of titanium deposited by pulsed magnetron sputtering: (a) 100 kHz; (b) 350 kHz (Arnell, Kelly, & Bradley, 2004)

Compared to the 350 kHz film, which is heavily pitted, the 100 kHz film is very smooth. This study showed that the variation of pulse frequency proposes a new method to control the ion current individually. Pulsing of a magnetron target can give orderly increases of energy and flux of the ions bombarding at the substrate. These variations can be seen through very substantial changes observed in the properties and structures of the

coatings. Many of the changes observed are dependent on frequency and certain properties can be optimized through the selection of a suitable frequency (Arnell *et al.*, 2004).

2.3.4 Magnetron Sputtering of Magnesium Oxide

T. Welzel *et al.* selected an Mg target material that was sputtered in an Ar/O_2 environment to study the full energy distribution of O^- and O_2^- ions in a pulsed magnetron discharge. This material was chosen due to the extremely high secondary electron emission coefficient of magnesium oxide which is also formed at the surface of the target. The experiment was performed under vacuum and was pumped down to a base pressure of 10^{-4} Pa through the combination of a rotary pump and a turbomolecular pump. A fixed mixture of 100 sccm Ar and 20 sccm O_2 working gas was used, resulting in a target that was fully poisoned (arcing). Consequently, the working pressure was adjusted to 0.4 Pa. The average discharge power used was 100 W with the frequency of one set ranging from 25-50 kHz and a second set frequency of 100 kHz. The deposition working distance was 100 mm. The conclusions of the experiment showed that long 'off' times slightly reduce the ion energy of the mid-energy ions. However, insulating material substrates are often at floating potentials which means the potential of the surface floats with changes in the ion energies and the plasma potential. Even in the mid-energy range ion energies will typically stay unaltered by the modulation in potential (Welzel *et al.*, 2011).

CHAPTER 3

MATERIALS AND METHODS

3.1 Manufacturing and Characterization Techniques

3.1.1 Magnetron Sputtering

In this study, the AJA International, Inc. ATC 1800 F magnetron sputtering system was used. The system includes three sputtering guns and can be used for DC (1000 W max), Pulsed DC (5000 W max) or RF (500 W max) sputtering applications (Figure 3.1).

Figure 3.1. AJA 1800F Magnetron Sputtering System at NCAT

The substrate holder can control the distance between the substrate and the target through an adjustable stage and uniform thicknesses can be achieved through the rotation of the substrate holder. Substrates can be quickly maneuvered into and out of the deposition chamber without losing high vacuum due to a turbomolecular pump. The system also includes a residual gas analyzer (RGA) that provides a detailed gas analysis of the system. The RGA gives an accurate representation of the moisture level and other impurities that may be in the deposition chamber. Monitoring the RGA allows replication of the same operating conditions in the deposition processes and also optimization of these processes.

All the depositions done in this study had a constant argon flow rate of 20 sccm, working distance of 85 mm and were performed at room temperature. All MgO depositions were done with a 99.5% Mg target using PDC and reactive sputtering.

3.1.2 Stylus Profilometry

Single layer thicknesses were measured using the KLA Tencor Alpha-Step IQ Surface Profiler. This system is a high-sensitivity, computerized surface profiler that measures waviness, roughness and step height in various applications. It has the ability to measure micro-roughness over short distances and allows measurement of vertical features from under 0.4 µin. (100 Å) to approximately 0.4 mm. As a result of these features, the noise from the measurement data is very minimal thus resulting in more accurate readings. The vertical resolution of the profiler is 0.012 Å or 0.24 Å. The profilometer, Figure 3.2, is capable of repeating scans up to 10 times and it can also automatically average data.

Figure 3.2. KLA Tencor Alpha-Step IQ Surface Profiler

The Alpha-Step IQ has the ability to level and fit data, which allows accurate measurements of curved surfaces. The horizontal resolution is not limited by the number of data points but by the radius of the stylus and the minimum spacing required between two data points is 0.01 µm. Sample sizes up to 150 mm (6 in.) wide and 21 mm (0.83 in.) thick can be accommodated and the equipment can also be used for verification and calibration purposes. As the stylus scans across the sample, an analog signal is generated, converted into a digital signal, stored, analyzed (Wikipedia, 2011) and then a plot is formed. The digitized data signal, as seen in Figure 3.3, permits precise and easy quantification of results. In this study, the profilometer was not only used for measuring single layer thicknesses but for calibration and verification experiments as well.

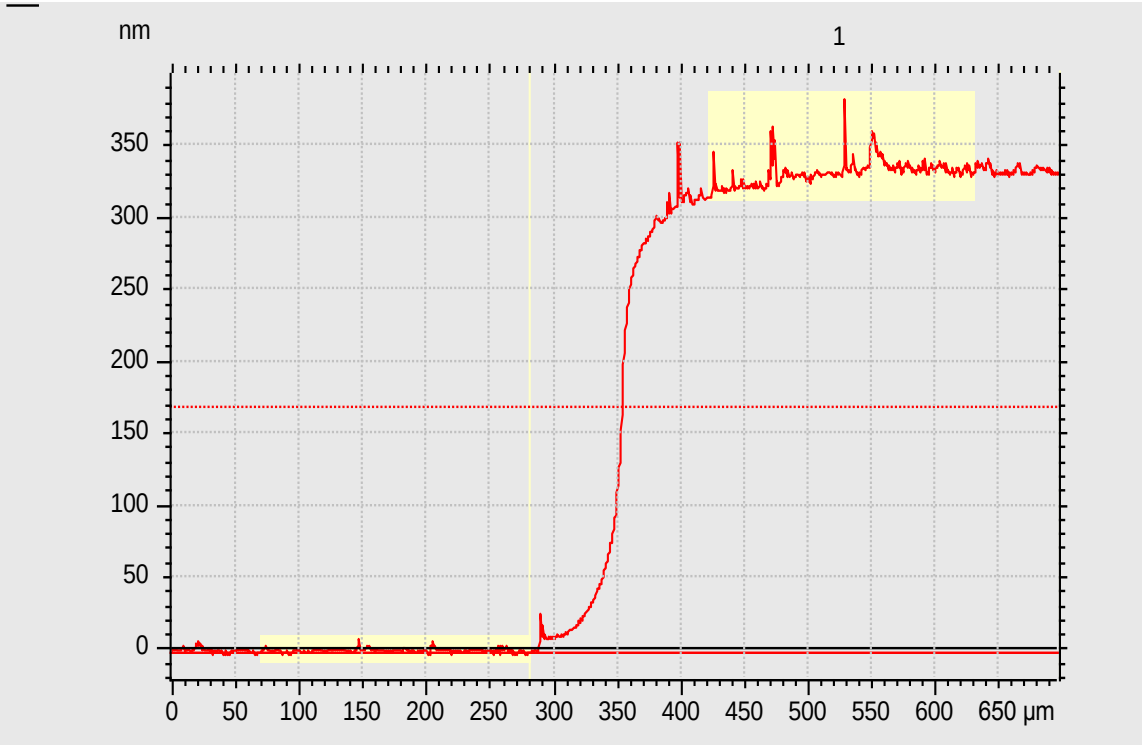

Figure 3.3. Typical output of surface profile data from KLA Tencor Alpha-Step IQ Surface Profiler

3.1.3 X-Ray Diffraction (XRD)

The XRD system used in this study was the Bruker AXS D8 Discover (Bruker AXS, 2011) This XRD is suitable for low-angle X-ray reflectometry (XRR), high angle high resolution diffractometry, both thin and bulk film powder and also has an adjustable knife-edge collimator for use in high resolution reflectometry for thin film structure (roughness, density, thickness) (University at Albany State University of New York, 2011). XRR is a technique that is non-destructive and is excellent for studying thin film structures with very low layer thicknesses. The XRD (Figure 3.4) is equipped with advanced X-ray detectors and was used to determine the crystallographic structure and orientation of the samples.

Figure 3.4. Bruker AXS D8 Discover X-ray diffractometry system at NCAT

Multilayered samples were analyzed with XRR and LEPTOS 5.02 software, which provides various approaches for evaluating data measured by enabling simple first guesses of the physical parameters of samples or through sophisticated modeling of samples. In the estimate mode, evaluation of the sample parameters can be done quickly through simple analytical formulas. Layer thicknesses can be evaluated through the estimate mode without fitting the data sets. In the fit mode, which was used for measuring multilayered samples in this study, the experimental data is accurately fit using non-linear fitting algorithms (Bruker AXS, 2008).

3.1.4 Scanning Electron Microscopy

In this study, the Hitachi SU8000 Field Emission Scanning Electron Microscope (SEM) was used. Figure 3.5 shows the SU8000 which features a semi-in-lens objective lens along with a top detector.

Figure 3.5. Hitachi SU8000 Field Emission Scanning Electron Microscope

Optimum contrast visualization of signals generated from samples is achieved through the combination of the top detector with the conventional upper detector technology. These signals include high-angle backscattered electrons, low-angle backscattered electrons and secondary electrons (SE). High-angle backscattered electrons at low accelerating voltages can be detected using the top detector. The compositional

contrast of the top surface of the sample can be seen with this imaging component. Information from the sample's shallow surface can be visualized at 100 V through the capturing of SE signals by the top detector. An upper detector is also included and provides a high efficiency SE detection signal. This allows high-resolution imaging of the structure of the surface (Hitachi High-Technologies, 2008).

3.1.5 Optical Microscopy

The optical microscope used in this study was the Axio Imager.M2m Upright Microscope by Carl Zeiss. The Imager.M2m (Figure 3.6) allows the specimen to be seen in darkfield and brightfield with minimized stray light that is practically aberration-free.

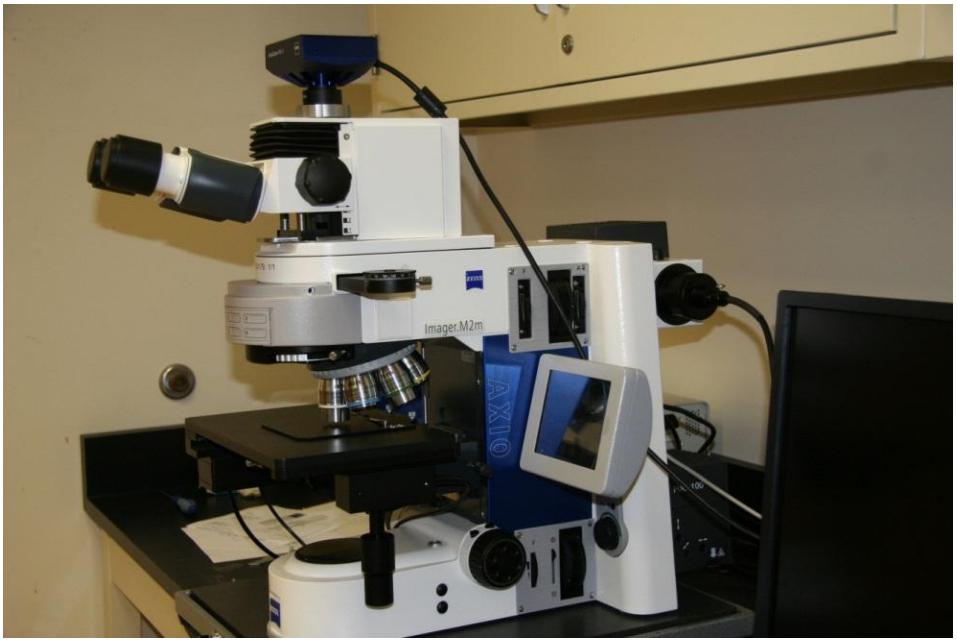

Figure 3.6. Zeiss Axio Imager.M2m upright optical microscope

CHAPTER 4

EXPERIMENTS AND MEASUREMENTS

4.1 Cu Deposition on Mg Screw

In this experiment a 99.995% Cu target was used to deposit on a 99.5% Mg screw at room temperature with a DC power source. The screw was placed on a custom made stage, Figure 4.1b, and Cu was deposited on the Mg screw with a substrate rotation speed of 30 rpm as seen in the schematic representation in Figure 4.1a.

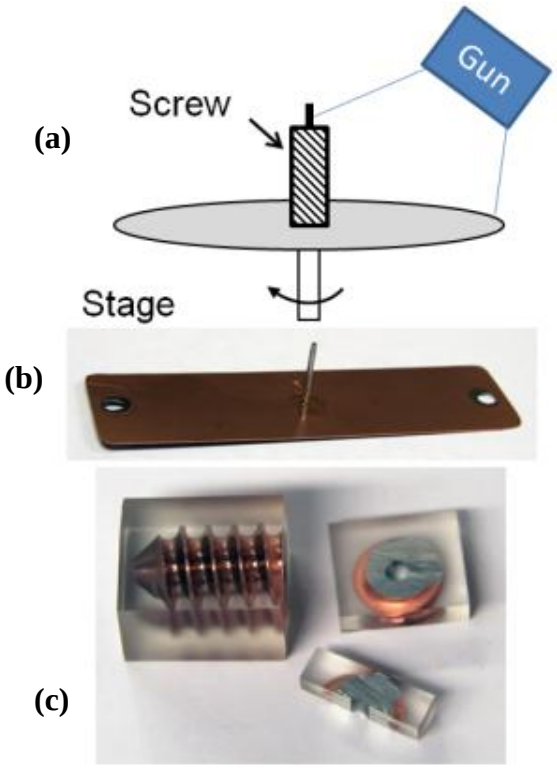

Figure 4.1. (a) Schematic of 3D coating method, (b) stage for 3D coating and (c) coated sample in epoxy resin and its cuts

After this deposition the screw was removed from the chamber, flipped over, and another deposition was performed for an additional hour. Once the deposition was complete, the coated screw was set in epoxy and cured overnight. The screw was then cut along the threads with an Allied High Tech Products, Inc. TechCut 5™ Precision Sectioning Machine and those pieces were cut in half (Figure 4.1c). The screw pieces were polished down to 1 µm diamond grit size, SEM images were taken and EDS analysis was performed.

4.2 Optimization of MgO Deposition

In PDC reactive depositions of metal oxides with pure metallic targets, different parameters such as power, frequency, oxygen content and gun position must be considered. Two gun positions, 6 mm and 7 mm, were considered for the gun position calibration (Figure 4.2).

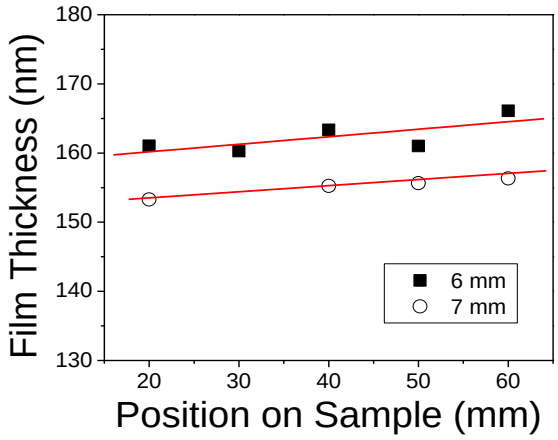

Figure 4.2. Magnetron sputtering gun position calibrations

Calibration samples were used to determine deposition parameters. The substrates used in these depositions were rectangular glass microscope slides 75 mm by 25 mm and were chemically cleaned with acetone and ethanol respectively. Height measurements were done using the profilometer and deposition rates were calculated using the formula shown below.

$$Rate\ \left(\frac{nm}{s}\right) = \frac{Thickness\ (nm)}{Deposition\ Time\ (s)}$$

Two gun positions, 6 mm and 7mm, were chosen and five depositions were done at each gun position. A step was created by placing a piece of tape on the glass substrate, along the width, prior to deposition. Height measurements of each sample were done using the profilometer. Average thicknesses of the samples were calculated for each gun position and these average thickness values were used for calculating the rate. This calibration data was used to determine an optimum gun position. Table 4.1 shows two out of the ten total samples that were used for gun position calibration.

Table 4.1. Deposition parameters for the gun position calibrations

Sample No.	Material	Power (W)	Pressure (mT)	Duration (s)	Average Thickness (nm)	Rate (nm/s)
1	Mg	75	3	600	152	0.25
2	Mg	75	3	600	157	0.26

Once the gun position was chosen, oxygen calibration took place. This was done by gradually increasing the oxygen flow rate while keeping the argon flow rate at a constant 20 sccm (Table 4.2). Figure 4.3 is a graphical representation of the effects of increasing oxygen in the deposition chamber and its effects on the deposition rate.

Table 4.2. Deposition parameters for the samples used for oxygen content calibration

Sample No.	Material	Pressure (mT)	Oxygen (sccm)	Oxygen (%)	Duration (s)	Thickness (nm)	Rate (nm/s)
3	Mg	4	0	0	600	145	0.24
4	MgO	4.2	1	5	600	151	0.25
5	MgO	4.4	2	10	600	110	0.18
6	MgO	4.6	3	15	600	86	0.14
7	MgO	4.8	4	20	600	77	0.13

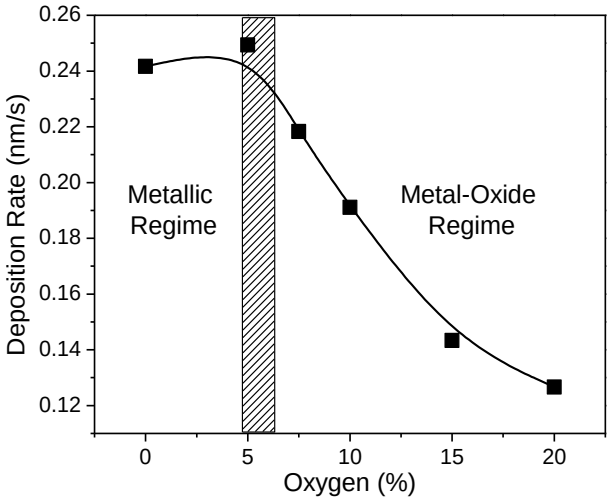

Figure 4.3. Effect of oxygen content on MgO PDC deposition rate.

From the data presented in Table 4.2 and Figure 4.3, an oxygen flow rate of 1.5 sccm (7.5%) and a pressure of 4.3 mT were chosen. Figure 4.4 shows the effect of an increasing water pressure in the deposition chamber and its effects on deposition rates.

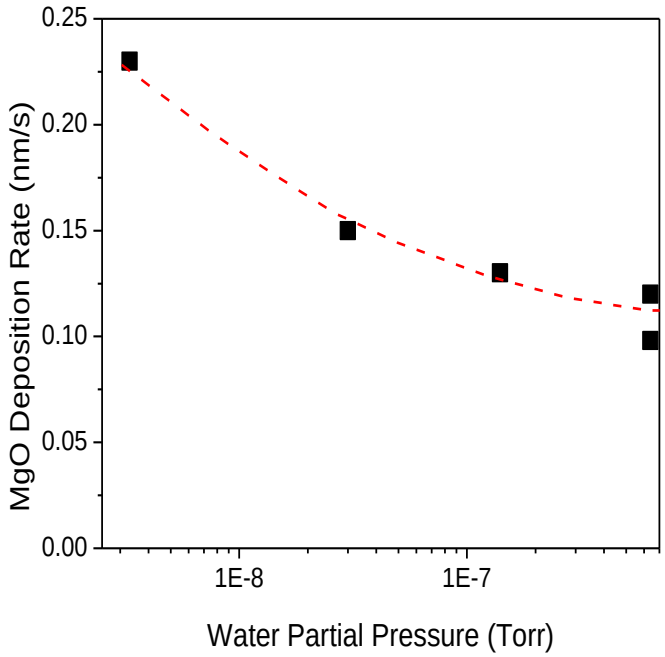

Figure 4.4. Effect of water vapor pressure in chamber on MgO PDC deposition rate

The residual gas analyzer (RGA) mass spectrometer was used to monitor the partial water pressure in the deposition chamber. Prior to each MgO deposition, the RGA scan was run and the partial water pressure was recorded. Frequency calibrations from 50 kHz to 350 kHz were performed and height measurements were taken. The rate was calculated for each sample and these rates were plotted with respect to the corresponding frequency. The frequency calibration showed that the partial water pressure had a

significant effect on the deposition rates as was also seen in Figure 4.4. Figure 4.5 shows the frequency calibration and the inconsistency in the rate shows that the partial water pressure had a significant effect on the deposition rates as well as in the determination of an optimum frequency solely based on this figure.

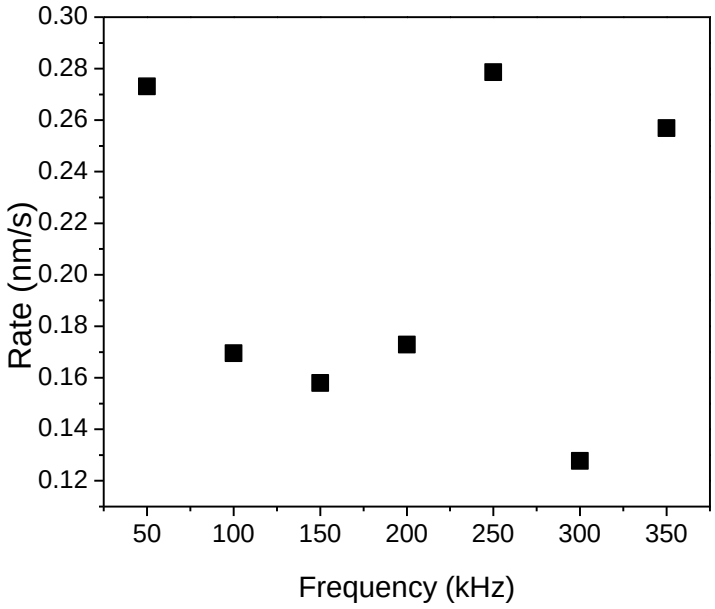

Figure 4.5. Effect of PDC frequency on MgO deposition rate

The observation from these two figures led to two solutions being developed in order to combat the issue of increasing water pressure. These two solutions are detailed in section 5.2. From the literature (Arnell *et al.*, 2004), prior PDC deposition experience and frequency calibrations, the midrange frequencies of 100 kHz-300 kHz, produce the best deposition rates. From this, an optimum frequency of 250 kHz was chosen.

4.3 Mg-MgO-Cu System

In order to evaluate whether MgO was an applicable material to use as an interface layer for Mg screws and Cu coatings multilayered systems were created using these three materials. Mg and Cu thicknesses were kept at a constant 30 nm while the MgO thickness varied from 10-100 nm. The substrate used for these depositions were 22 mm x 22 mm Thermo Scientific microscope cover glasses. PDC was used for Mg and MgO depositions and DC was used for Cu depositions. Prior to the depositions, the substrates and pieces were cleaned in a TePla M4L RF Gas Plasma System for 20 minutes. These samples are shown below in Table 4.3.

Table 4.3. Deposition parameters for Mg-MgO-Cu samples

Sample No.	Material	Power (W)	Base Pressure (mT)	Pressure (mT)	Oxygen flow rate (sccm)	Duration (s)	Frequency (kHz)	Estimated Thickness (nm)
42	Mg,Cu	100	2.3E-7	4	0	95,165	250	30,30
43	Mg,MgO,Cu	100	1.5E-7	4,4.3,4	0,1.5,0	95,30,165	250	30,10,30
44	Mg,MgO,Cu	100	2.3E-7	4,4.3,4	0,1.5,0	95,60,165	250	30,20,30
45	Mg,MgO,Cu	100	2.0E-7	4,4.3,4	0,1.5,0	95,90,165	250	30,30,30
46	Mg,MgO,Cu	100	2.2E-7	4,4.3,4	0,1.5,0	95,145,165	250	30,50,30
47	Mg,MgO,Cu	100	1.7E-7	4,4.3,4	0,1.5,0	95,290,165	250	30,100,30
48	MgO,Cu	100	1.5E-7	4.3,4	1.5,0	290,165	250	100,30
49	Cu	100	2.2E-7	4	0	165	250	30

XRR was performed and height measurements of the multilayered systems were measured using the LEPTOS 5.02 software. A sample model was created using the software's material database to select different materials for each layer and the estimated thickness and roughness values were input for simulation purposes. The peaks on the plot were automatically recognized using the peak search tool and were relabeled as fringes. In order to theoretically simulate the experimental conditions of the X-ray scattering of the samples, a simulation had to be performed. Once the simulation was performed, the measured data was overlaid onto the simulation as seen in Figure 4.6.

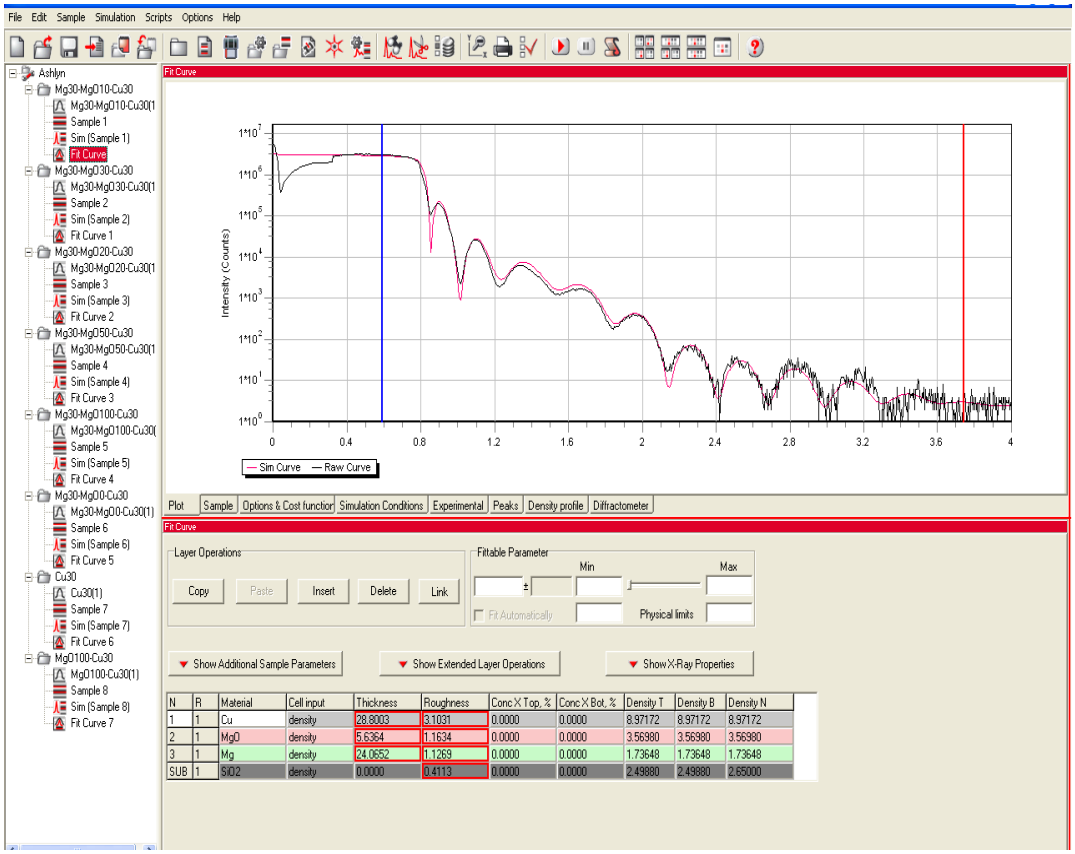

Figure 4.6. An example of XRR data fitting for sample 42 (screenshot from Leptos 5.02 Software)

The “Fit Automatically” box was checked for the thickness and roughness values of each layer and the minimum and maximum physical boundaries of these parameters were set by the user. Once a red rectangle appeared around a certain parameter, it was automatically fit as seen above, in Figure 4.6, for the thickness and roughness values. The Fittable Parameter group provided a manual mode and a slider was used to observe the resulting changes in the positions of the thickness fringes by moving the slider to the left and the right. Overlaying the measured data directly onto the simulated curve was done through the fitting procedure until the best fit possible was achieved. Thicknesses were measured from achieving the best possible fit. The Axio Imager.M2m Upright Microscope was used to observe the samples deposited on the broken glass pieces.

4.4 Mg-MgO System

In this section, Mg-MgO systems were deposited on various glass substrates and immersion tests were performed using optical methods. Samples were also deposited on silicon substrates for XRD and SEM analysis. The effect of different solutions, such as albumin, saline, PBS and cell culture media, on the Mg-MgO systems was also studied. Mg-MgO systems were deposited on whole and broken 22 x 22 mm Thermo Scientific microscope cover glasses pieces and thickness evaluation was performed using the XRR method. Table 4.4 shows the deposition parameters for these immersion test samples and the thickness values. Figure 4.7 is an example of thickness analysis done by LEPTOS 5.02 software with the black curve representing the raw data and the red curve being the simulation.

Table 4.4. Deposition parameters for Mg-MgO samples

Sample No.	Material	Pressure (mT)	Oxygen flow rate (sccm)	Duration (s)	Thickness (nm)
50	Mg	4	0	95	26
51	Mg,MgO	4, 4.3	0,1.5	95, 30	6
52	Mg,MgO	4, 4.3	0,1.5	95, 60	13
53	Mg,MgO	4, 4.3	0,1.5	95, 90	18
54	Mg,MgO	4, 4.3	0,1.5	95, 145	23
55	Mg,MgO	4, 4.3	0,1.5	95, 290	55

Figure 4.7. An example of XRR data fitting for Mg-MgO sample 53 (screenshot from Leptos 5.02 Software)

Initial immersion tests were performed on Mg-MgO samples, deposited on the 22 x 22 mm glass, using PBS and deionized water at room temperature and the optical microscope. Transmitted light was used and images of the samples were taken manually. This same test was repeated with an EOS 20D Canon Camera and a Logan Desk Top

Light Box. 15 mm diameter circular Fisherbrand cover glass substrates were used for the Mg-MgO depositions. 5 samples of each sample, listed in the Table 4.5 below, were made and placed in a Corning Costar 24-well cell culture plate.

Table 4.5. Mg-MgO coating deposition parameters for samples tested in different media

Sample No.	Material	Power (W)	Base Pressure (mT)	Pressure (mT)	Oxygen Flow Rate (sccm)	Duration (s)	Frequency (kHz)	Estimated MgO Thickness (nm)
79	Mg,MgO	250	7.1E-7	4.5	2.5	51	250	30
80	Mg,MgO	250	3.8E-7	4.5	2.5	86	250	50
81	Mg,MgO	250	4.5E-7	4.5	2.5	170	250	100
82	Mg,MgO	250	1.8E-7	4.5	2.5	254	250	150
83	Mg,MgO	250	3.8E-7	4.5	2.5	339	250	200

All of the solutions used in this immersion test were first put into an incubator for some time until the solutions reached 37ºC. The albumin used was 5% Bovine Serum Albumin in Dulbecco's Phosphate Buffered Saline (DPBS). The PBS used was the same as the previous immersion test. The media was a 1:1 mixture of Ham's F12:Dulbecco's Modified Eagle's Medium and the second media solution contained 10% fetal bovine serum (FBS). The saline was a 0.9 wt.% NaCl physiological solution.

The samples were arranged as seen in the schematic, Figure 4.8, below. All the immersion test data was analyzed using Image-Pro Plus 6.0 software.

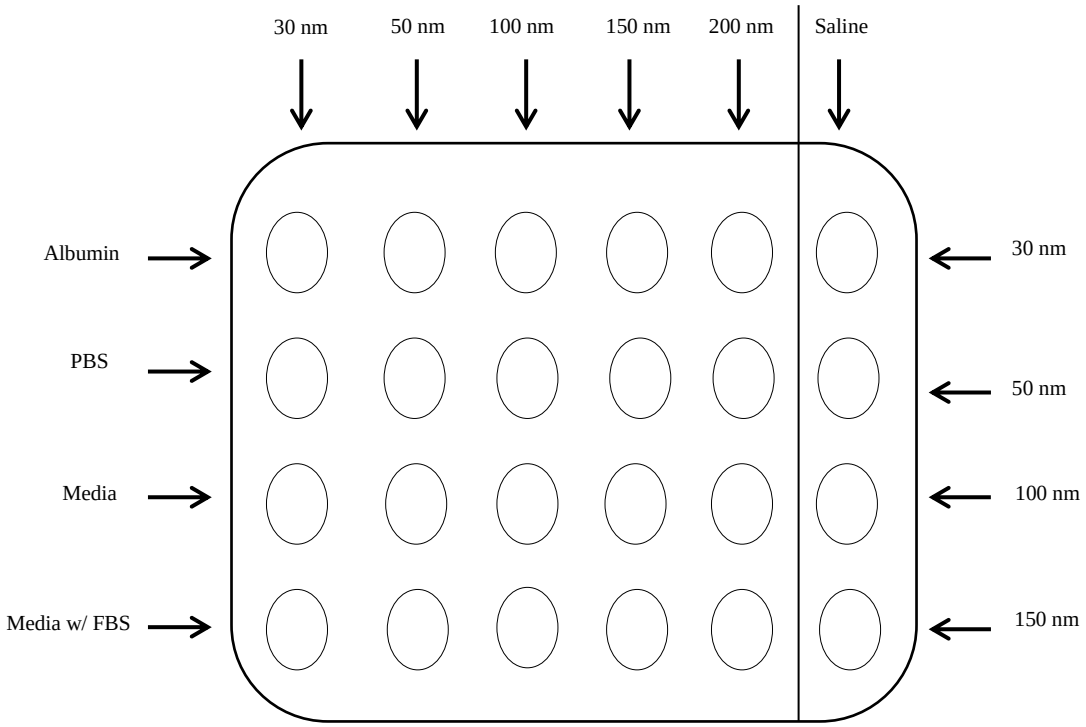

Figure 4.8. Schematic of sample placement on a 24-well plate for an immersion test in different media

The camera was setup on a tripod so that the camera was looking directly down on the well plate. The well plate was placed on the light box with the excess light being blocked with cardboard. 1 mL of each solution was placed into the proper wells and pictures were initially taken every minute, with the time increment gradually increasing depending on how fast the material degraded. The temperature was kept at a constant 37ºC. After each image was snapped, the well plate was placed back in the incubator so

the temperature could be maintained throughout the test. This data was analyzed in the same manner as the immersion test mentioned previously in this chapter.

4.5 Biocompatibility Testing of MgO

Thickness calculations for biological testing were done based on the results of the Mg-MgO immersion tests done in PBS at room temperature in the previous section. The results of the immersion test showed an increase in the deposition rate was necessary to achieve reasonable deposition times. Figure 4.9 shows that a deposition rate of 0.59 nm/s can be achieved with a power setting of 250 W.

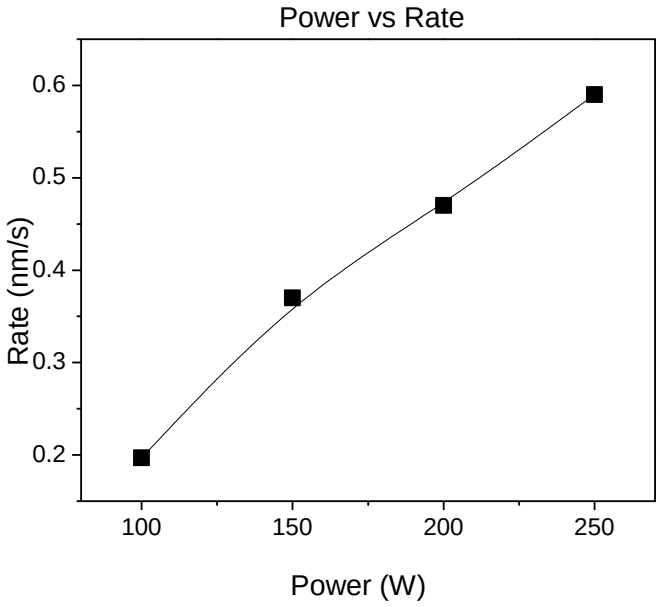

Figure 4.9. Effect of source power on PDC deposition rate of MgO

With this change in power the oxygen flow rate was increased to 2.5 sccm and the partial pressure increased to 4.5 mT due to recalibration based on the new power setting (Table 4.6).

Table 4.6. PDC deposition rate calibrations at different power

Sample No.	Material	Power (W)	Base Pressure (mT)	Pressure (mT)	Oxygen Flow Rate (sccm)	Duration (s)	Thickness (nm)
74	MgO	250	1.8E-7	4.5	2.5	180	106
75	MgO	250	1.2E-7	4.5	2.5	1115	658
76	MgO	250	1.4E-7	4.5	2.5	1902	1122
77	MgO	250	2.1E-7	4.5	2.5	4732	2792
78	MgO	250	1.4E-7	4.5	2.5	11781	6951

Since these samples were transparent, extra care was taken to ensure that the samples were not flipped over during transport from the substrate holder into the well plates. Identical samples, with a layer of Mg underneath, were made and the same cell adhesion assay was performed on these samples. This was done so that there was a visual indication of when the MgO had completely degraded and the solution had reached the layer of Mg underneath. Prior to deposition, the glass substrates were plasma cleaned for

20 minutes and then deposited on the 15 mm diameter substrates. The samples were then placed in the 24-well plates as seen in Figure 4.10 below.

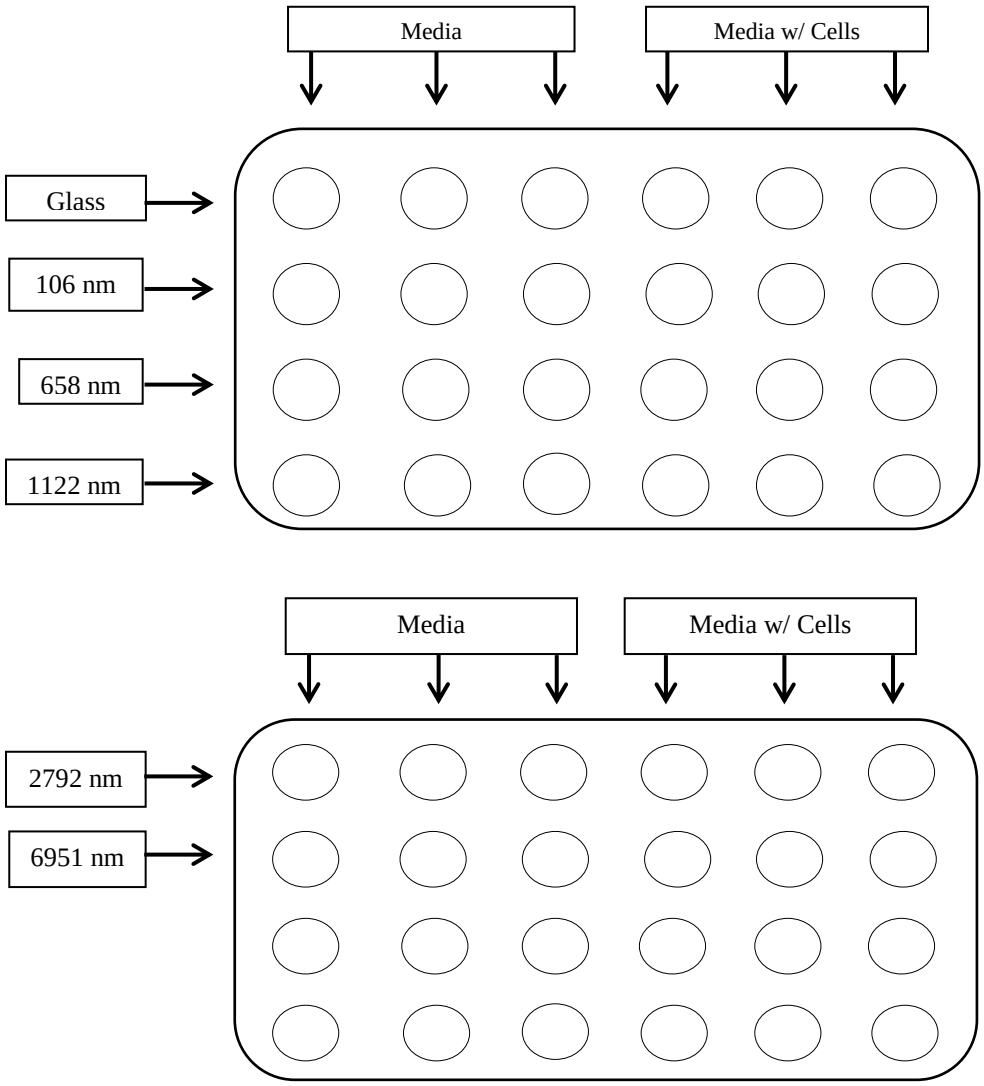

Figure 4.10. Configuration of sample placement on 24-well plates for cell viability tests

The human osteoblast cell line, hFOB 1.19 (ATCC), was maintained in a 1:1 mixture of Ham's F12:Dulbecco's Modified Eagle's Medium, supplemented with 0.3 mg/ml Gentamicin and 10% heat-inactivated FBS at 33.4^{o}C, under humidified air

containing 5% CO_2 for proliferation. Once the cells had approximately reached 90-100% confluency in T-75 cm^2 flasks, the culture medium was removed and the cell surfaces were washed with HBSS to remove serum, which contained trypsin inhibitor. Next, 0.25% Trypsin-0.53 mM EDTA solution was used to release the cells from the culture vessel by incubating the cells for 5 minutes at 37^oC. The reaction was stopped by adding an equal volume of ice-cold serum or serum-containing medium. The cells were collected by gently aspirating them into sterile 50-ml conical tubes. Propagation medium was used to wash the cells twice and were then collected through centrifugation at 1,000 rpm at 4^oC. Cell viability and concentration was determined using a hemacytometer and Trypan Blue Dye, respectively. The cells were then immediately used for sub-culturing, experimental investigations, or dispersed into one-milliliter aliquots (5 x 10^6 cells/ml) in freezing medium (80% propagation medium, 10% serum, 10% DMSO) and placed into cryopreservation tubes. The cells in the freezing medium were kept overnight at -80^oC and then placed in liquid nitrogen for long-term storage.

For sub-culturing, 10^4-10^5 cells were placed into new flasks containing 15 ml propagation medium, renewed every 2-3 days, and cultures were maintained as previously mentioned. For experimental investigations, i.e., adhesion assays, 5 x 10^5 cells were plated in the 24-well plate as seen in Figure 4.10. The cells were placed in the incubator for 4 hours and an EVOS phase contrast inverted microscope was used to evaluate cell adhesion. Each experimental condition was performed in triplicate and cell attachment was recorded as percent confluency compared to the glass substrate controls.

At the end of the experiment, the media was removed and the surface of the materials were washed with PBS and then aspirated.

CHAPTER 5

RESULTS AND DISCUSSIONS

5.1 Cu Deposition on Mg Screw

The purpose of this study was to establish a technique for the uniform deposition of a metallic coating on an Mg screw. The results of this study indicate this is a plausible and effective way to achieve uniform thicknesses on complex geometries such as screws. Cu was chosen as a coating in this case because of its cytotoxic properties and because of its contrasting color with Mg. Upon further inspection, SEM images revealed accelerated corrosion due to galvanic contact between the metallic coating and the metallic substrate (Figure 5.1).

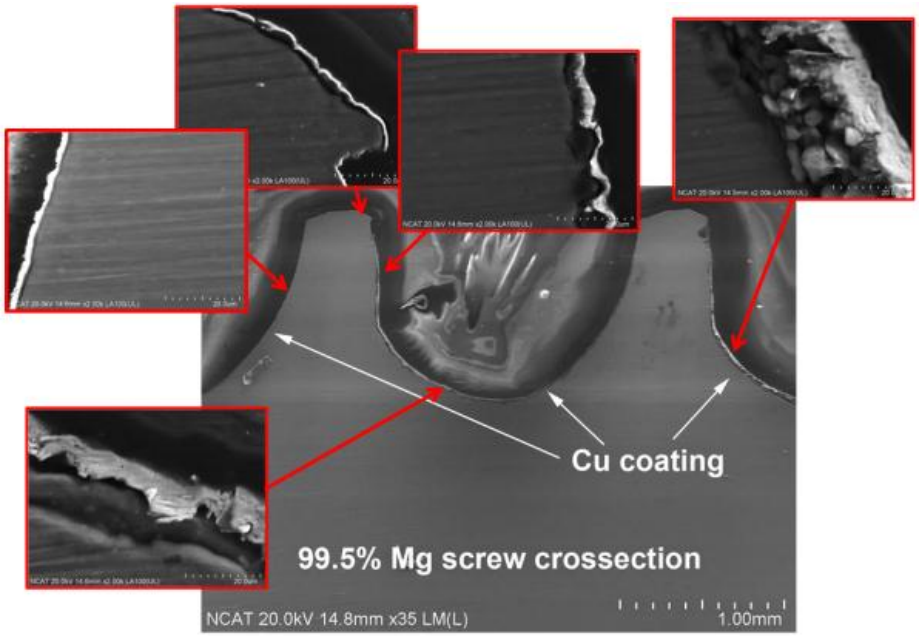

Figure 5.1. Cross sections of the Mg screw coated with 2 µm thick Cu

This accelerated corrosion of the more active metallic component caused a loosening of the interface between the substrate and the coating and also caused rapid degradation. Since the difference in the electrochemical potentials of Mg and Cu is so significant, avoiding contact with electrolytic media is critical with both metallic parts. Though the cross sectional polished surfaces indicate a continuous Cu coating (Figure 5.1), it was quickly delaminated from the Mg substrate due to accelerated corrosion. In order to address this galvanic contact, an interface layer of MgO was introduced between the metallic coating and the metallic substrate (Figure 5.2).

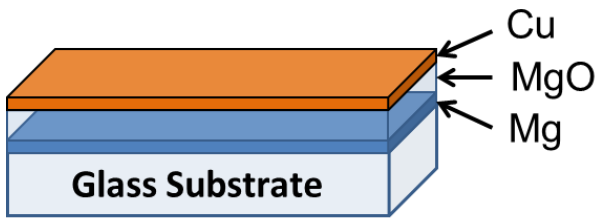

Figure 5.2. Schematic approach of a metal on metal coating stabilized with MgO as a galvanic separator

5.2 Optimization of MgO Deposition

An unforeseen issue that occurred during the optimization of MgO was the effect of increasing partial water vapor pressure on deposition rates. The water pressure was recorded prior to each deposition using the RGA mass spectrometer. Table 5.1 shows the samples, which were deposited consecutively, while the graphical representation, Figure 5.3, shows the highest deposition rates for the MgO samples was achieved immediately after the Mg deposition. Throughout the depositions of the remaining MgO samples, the

water pressure gradually increased which caused the deposition rates to gradually decrease.

Table 5.1. Effect of water pressure on rate

Sample No.	Material	Base Pressure (mT)	Duration (s)	Average Thickness (nm)	Deposition Rate (nm/s)	Water Pressure (mT)
32	Mg	6.7E-07	300	79	0.26	6.6E-08
33	MgO	5.2E-07	300	70	0.23	3.3E-09
34	MgO	6.7E-07	300	45	0.15	3.0E-08
35	MgO	8.2E-07	300	40	0.13	1.4E-07
36	MgO	1.2E-06	300	35	0.12	6.4E-07
37	MgO	1.3E-06	300	29	0.10	6.4E-07

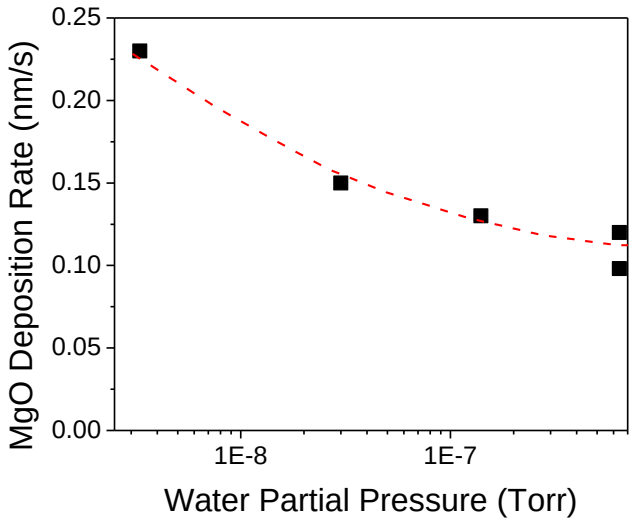

Figure 5.3. Effect of water vapor pressure in chamber on MgO PDC deposition rate

Two solutions were developed to combat the issue of increasing water pressure. The first solution was to do a short 5 to 10 minute Mg deposition before an MgO

deposition. The second solution was to use a liquid nitrogen cooled water trap ("cold finger"). Both of these techniques proved to be effective with the second solution being preferable, since it is not necessary to do additional depositions.

SEM images of the ~3 μm thick sample show that the coating was polycrystalline and had uniform crystallite sizes 80-100 nm. The SEM images also showed that the coating had no defects such as cracks or inclusions (Figure 5.4).

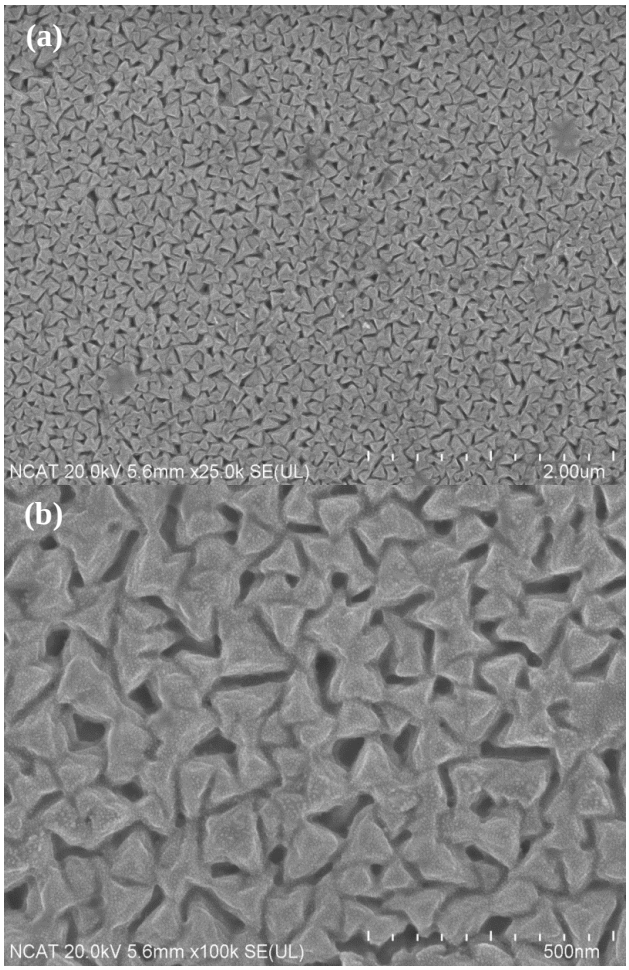

Figure 5.4. SEM images of ~3 μm thick MgO sample at magnifications 25k (a) and 100 k (b)

At high magnification (Figure 5.5), it was observed that the coating exhibited porosity with about 100 nm pores developing due to columnar growth. Thin films <200 nm did not have pores and this technique must be optimized further to avoid pores in thick (>1 µm) coatings.

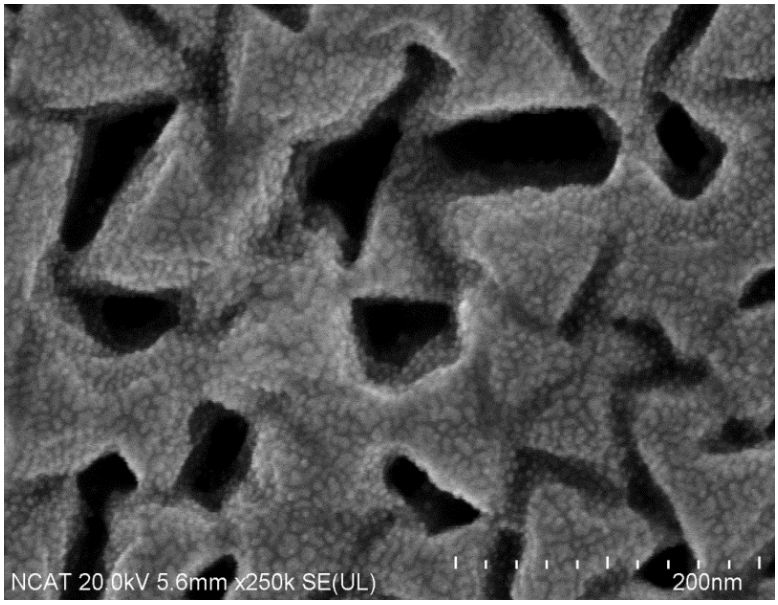

Figure 5.5. SEM image of ~3 µm thick MgO coating at magnification 250k (the small nanoparticles with size <5 nm is the gold coating deposited on the sample to avoid charging during SEM image acquisition)

X-ray diffraction patterns of all deposited MgO films exhibited two peaks corresponding to (111) and (222) diffraction planes in FCC cubic crystalline MgO (reference PDF card number 00-045-0946 in XRD database, Fm-3m, a = 4.212 Å) – Figure 5.6. The absence of other peaks in the XRD pattern indicates that MgO films have a preferred orientation along the (111) direction. This orientation typically leads to films with a columnar structure that corresponds to the SEM images of MgO thin films (Figures 5.4 and 5.5). An average grain size of about 50 nm was estimated from the width

of the diffraction peaks. This value is also in agreement with SEM observations. The lattice parameter is very close to powder data, assuming there are low stresses in the film. The width of the rocking curve suggests that variations in crystal orientation in the columnar structures can reach 10º. This number is also typical for polycrystalline columnar structures. Applying RF bias did not affect the grain size and orientation of the MgO films (Figure 5.6). From this it can be concluded that the optimization parameters used in this study and the PDC method of MgO depositions produced relatively rough, non-stressed, polycrystalline films that have marginal alignment in columnar structures.

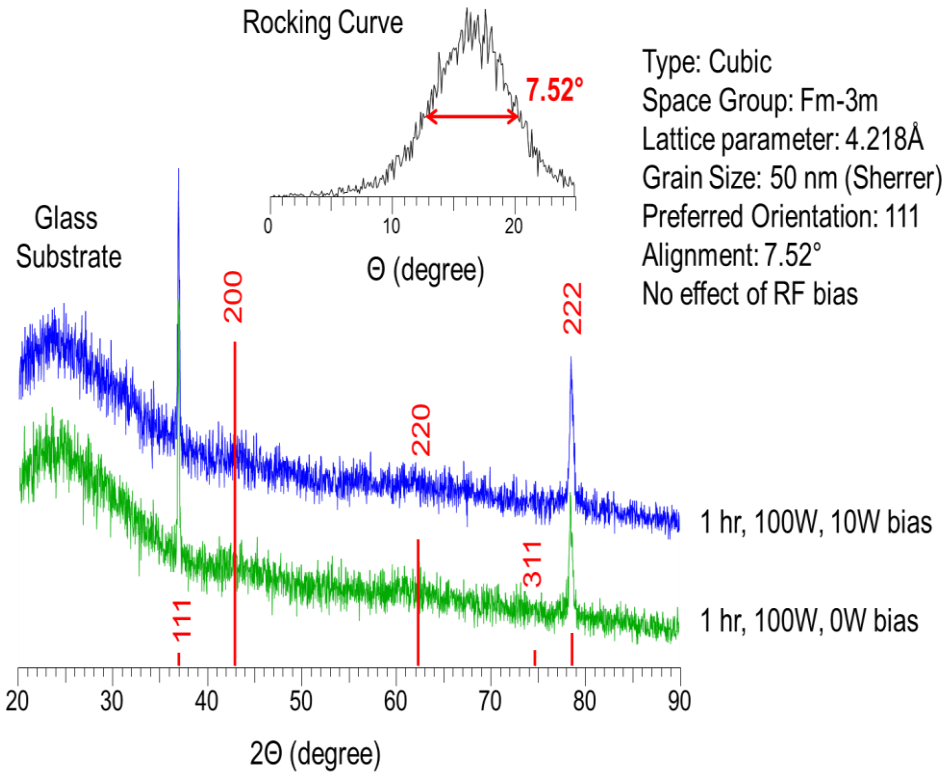

Figure 5.6. XRD analysis of 600 nm thick MgO thin films deposited with and without 10 W RF bias at room temperature

5.3 Mg-MgO-Cu System

The profilometer is not capable of measuring individual layers of multilayered samples, which is why X-ray reflectometry was used. Another method capable of evaluating individual thicknesses of every layer in multilayered coatings is elipsometry, however, this method is not available at NCAT. Table 5.2 shows 5 multilayered samples with estimated thicknesses calculated using the rates and the thicknesses calculated from XRR data using LEPTOS software.

Table 5.2. Comparison between estimated and measured thickness values

Sample No.	Layer #	Material	Estimated Thickness (nm)	Measured Thickness (nm)
43	1	Mg	30	24
	2	MgO	10	6
	3	Cu	30	29
44	1	Mg	30	23
	2	MgO	20	11
	3	Cu	30	27
45	1	Mg	30	23
	2	MgO	30	16
	3	Cu	30	29
46	1	Mg	30	23
	2	MgO	50	28
	3	Cu	30	27
47	1	Mg	30	22
	2	MgO	100	78
	3	Cu	30	23

The average measured value for Cu was 27 nm and 23 nm for Mg, which was not significantly different from the estimated 30 nm. However, the measured thicknesses of MgO were significantly less than the estimated thickness values. The description of the calculation procedure is given in section 4.3. MgO at certain thicknesses makes Cu stable. It was observed that MgO stabilized Cu at thicknesses greater than 50 nm and this also proved to be a sufficient galvanic separator between Mg and Cu. Embedding MgO can stabilize metallic layers such as Cu on top of metallic substrates, and this is why the effects of MgO are being studied.

5.4 Mg-MgO System

Mg-MgO two-layer thin films were deposited on glass substrates to evaluate MgO resorption rates in different media using immersion tests. Since MgO is transparent, a 30 nm layer of Mg was deposited underneath MgO to detect the removal of MgO by the optical immersion test method and to mimic the implant. At a 20 nm thickness, the Mg layer has an optical density around 0.6 D (or absorbs about 75% of light). This optical density is an acceptable absorbance to use for monitoring the process of corrosion *in situ*. It is evident that the corrosion process led to a reduction of the optical density of the samples. However, this reduction was delayed in samples with MgO coatings over the Mg layer compared to samples with just a layer of Mg. The results from this test show MgO dissolves in aqueous media approximately 3 times slower than pure metallic Mg. The results also show the corrosion rate of both Mg and MgO in deionized water is two

times slower than PBS. Figure 5.7 shows initial immersion test results with PBS and deionized water on samples with Mg and MgO thicknesses about 20 nm.

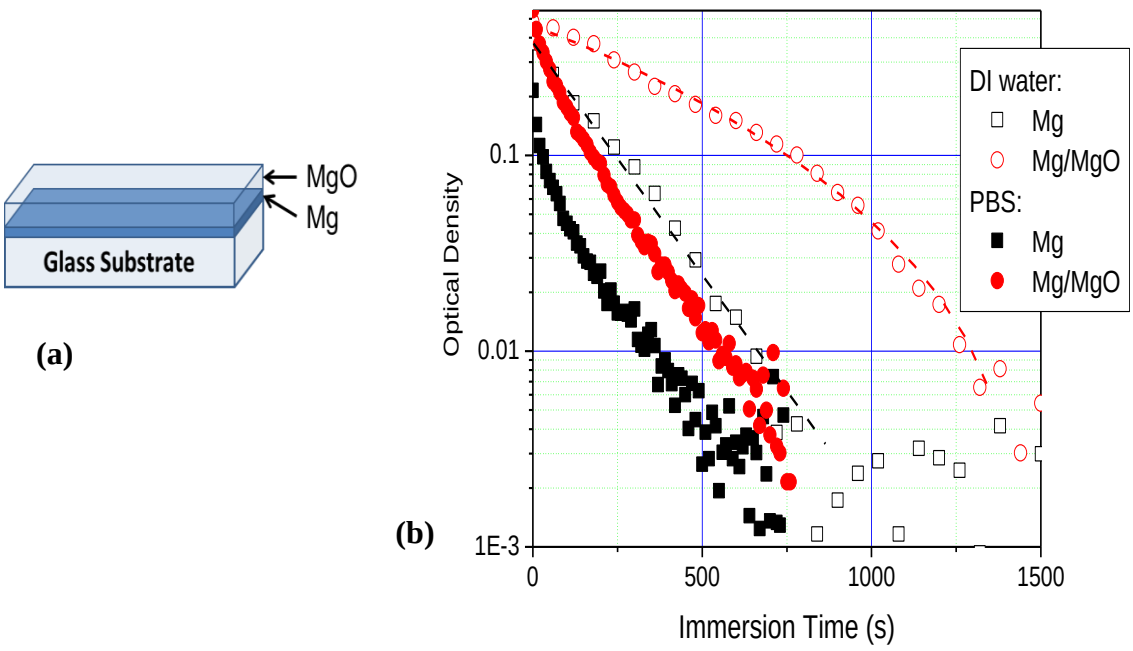

Figure 5.7. (a) Schematic of Mg-MgO sample, (b) Mg and Mg-MgO immersion test performed in deionized water and PBS at room temperature

This shows that the relative corrosion rates of Mg and MgO are sufficient for using thin layers of MgO as degradable galvanic separators between metallic substrates and coatings. Figure 5.8 shows the results of immersion tests performed with variable MgO thicknesses in PBS (Table 4.4). The initial optical density represents the absorbance of a ~25 nm thick Mg layer. Changes in optical density of the samples correspond to the changing thickness (or amount) of Mg in the sample.

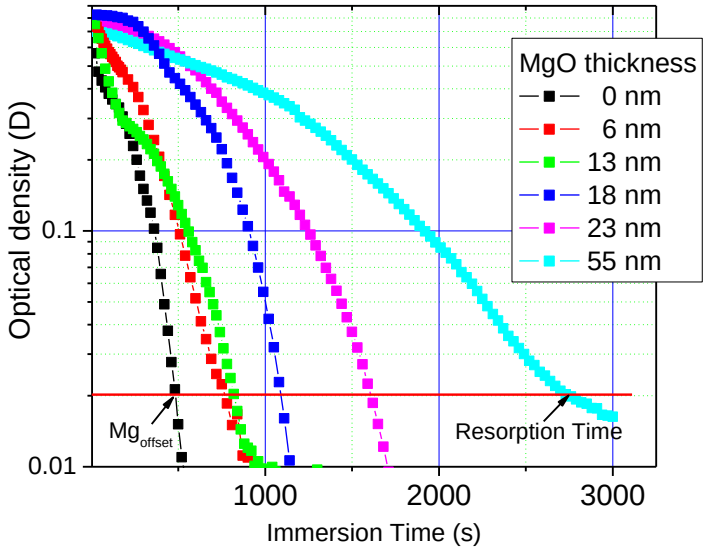

Figure 5.8. Semi-log plots of optical density of Mg-MgO samples vs. immersion time in PBS

At initial stages of degradation, MgO prevents access of aqueous media to the Mg layer and only a small change in optical density is reflected. The Mg layer is only affected by degradation at initial stages through pores and cracks in MgO. As the process progresses (MgO layer dissolves), the Mg layer becomes increasingly exposed to media and corrodes. When MgO is almost dissolved, Mg corrodes quickly which results in a relatively fast decrease in optical density. This approach allows the degradation rate of MgO to be evaluated. The red line in Figure 5.8 signifies an optical density of 0.02D which corresponds to a Mg layer thickness of about 1 nm. This is the optical density where we consider that both layers of coatings have completely degraded. Therefore, the time at which optical density reaches 0.02D can be considered as the resorption time of the two-layered system. The 25 nm thick Mg layer corrodes relatively quickly (Mg_{offset} =

484 s at a thickness of MgO equals 0). We can assume that the resorption time of MgO layers for every sample can be estimated using the following equation:

$$RT_{MgO} = RT - Mg_{offset}$$

where RT is the total resorption time of the sample. Figure 5.9 shows the resorption times plotted with respect to the thicknesses of MgO layers.

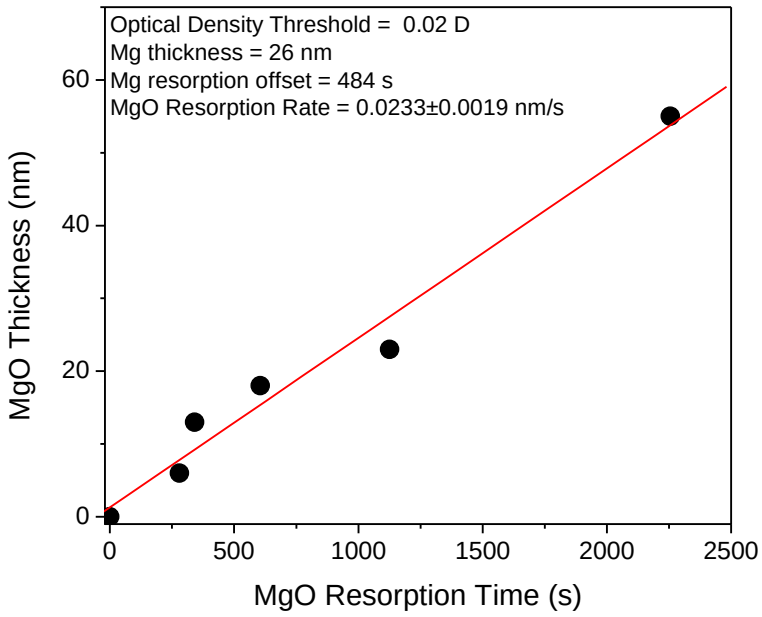

Figure 5.9. MgO resorption time based on MgO thickness

A linear dependence of MgO resorption times to the thickness of MgO layers suggests that the process of MgO degradation in PBS at room temperature does not depend on the amount of MgO dissolved in the media. In other words, the mechanism of MgO degradation in PBS can be described as a zero-order kinetics process. Therefore the slope of linear dependence between MgO thickness and resorption time represents the

degradation rate. Figure 5.9 shows that MgO dissolved in PBS at a rate of 0.023 nm/s and that at a 25 nm thickness MgO dissolved about 2.3 times slower than Mg (corrosion rate of Mg is 25/484 = 0.052 nm/s). We can conclude that zero order kinetics was observed at small MgO thicknesses (<60 nm). These numbers correlate with data received in preliminary tests shown in Figure 5.7. Figure 5.10 shows the resorption time of variable MgO thicknesses in different water-based media at 37ºC (samples 79-83, Table 4.5).

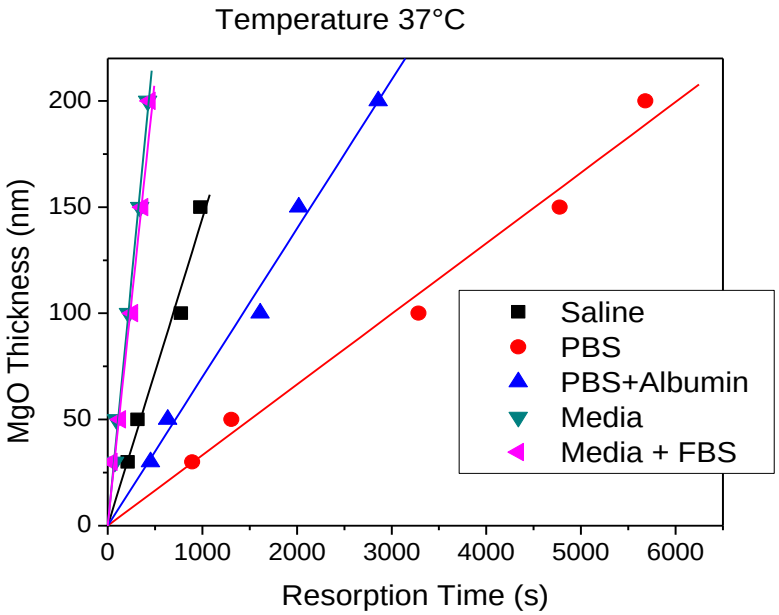

Figure 5.10. Resorption times of MgO in different solutions

The resorption rate of MgO has a strong dependence on the type of media (MgO dissolves in deionized water about 3 times slower than in PBS) and can be higher at physiological temperature (37°C) compared to room temperature. The motivation behind immersing Mg-MgO systems in different solutions was to use this methodology to

evaluate the resorption time of transparent coatings. As a result of this, this approach was extended to other water-based media. Figure 5.10 also shows a linear dependence and zero order kinetics. Variations in the slopes in Figure 5.10 indicate that the resorption rate of MgO varies significantly in different media. Figure 5.11 compares the stability of MgO in different solutions and at two different temperatures for PBS.

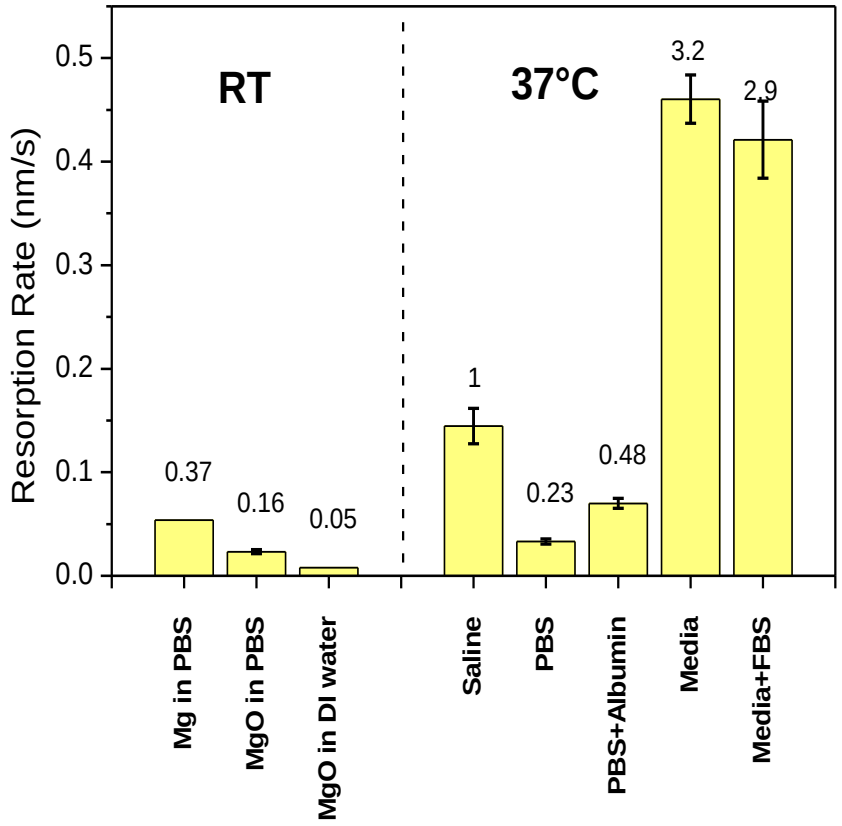

Figure 5.11. Resorption rates of MgO in different media at room temperature and 37°C

The numbers in the graph in Figure 5.11 show relative rates compared to the rate of saline at 37ºC. At 37ºC, the resorption of MgO in PBS is ~4.5 times slower than in saline. However, the addition of proteins increased the resorption rate more than 2 times. The 5% albumin in PBS solution exhibits a resorption rate only 2 times slower than saline. Moreover, media for the osteoblast cell viability test (see section 4.5) promotes dissolving of MgO – resorption rate in the media is 3 times higher than in saline. The effect of the media with FBS is similar to the media but exhibits a slightly slower resorption rate. The data shows that MgO dissolves in PBS ~15 times slower than the media. Taking into account that MgO dissolves in deionized water about 3 times slower than in PBS, the range of changes in resorption rates of MgO can reach 50-60 times depending on the water-based media used. Also, at 37°C, MgO dissolves in PBS about 1.5 times faster than at room temperature. These results show the importance of the resorption time studies for every media.

5.5 Biocompatibility Testing of MgO

In order to achieve reasonable deposition times for the desired resorption times, an increase in deposition rate was necessary. The use of higher deposition power (250 W *vs.* 100 W) in the PDC process is described in section 4.5. As a result, the rate increased from 0.20 nm/s to 0.59 nm/s and the deposition time for thick MgO films significantly decreased (Table 5.3). Figure 5.12 shows cell adhesion after a 4 hour incubation period with MgO-coated biomaterials.

Table 5.3. Deposition time before and after rate increase

Desired Resorption Time (hr)	Calculated Thickness (nm)	Deposition Time (hr)	
		at 100 W	at 250 W
1	100	0.2	0.05
4	650	0.9	0.3
6	1100	1.6	0.5
12	2800	3.9	1.3
24	7000	9.7	3.3

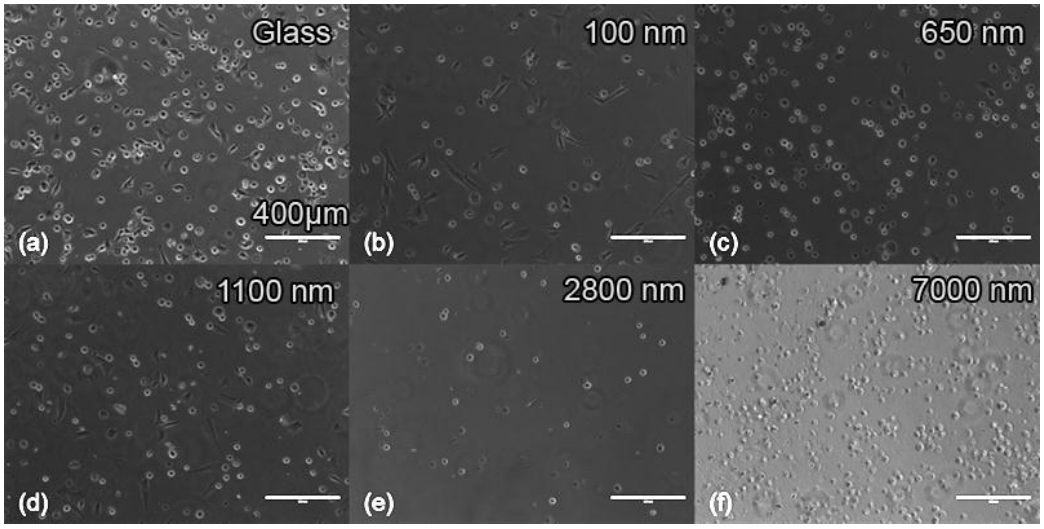

Figure 5.12. Cell adhesion on (a) glass control, (b) 100 nm MgO, (c) 650 nm MgO, (d) 1100 nm MgO, (e) 2800 nm MgO, (f) 7000 nm MgO

Figure 5.12a is the glass control which shows confluency around 50 – 60%, while Figures 5.12b and 5.12d show confluency around 20-30 %. In Figures 5.12c, 5.12e and 5.12f, little to no cell attachment is present. Figures 5.12b and 5.12c showed attachment to the glass substrate once the MgO had completely degraded away. Figures 5.12e and 5.12f show that MgO did not completely degrade, so the cells were not able to attach to the glass substrate as seen in the other figures. This cell adhesion assay showed that the

thinner MgO coatings were less toxic and that future efforts should be focused on coatings less than 1100 nm.

CHAPTER 6

CONCLUSIONS

Magnetron sputtering was used to produce uniform coatings on three-dimensional shapes, such as surgical screws, in order to achieve stable metallic coatings on Mg-based implants. SEM images were used to analyze the substrate and coating interaction and it was found that significant galvanic corrosion and coating delamination occurred. As a result of this, an intermediate layer of MgO was proposed as a galvanic separator between metallic substrates and coatings. Systematic studies of the deposition process, characterization and the properties of MgO coatings led to the following conclusions:

1. The magnetron sputtering system at NCAT can produce uniform coatings on three dimensional shapes.
2. Galvanic separators between the metallic substrate and metallic coating can help to produce stable metal on metal coatings with predictable properties. MgO was chosen as a separator material for the new generation of Mg-based metallic implants because of its biocompatibility and degradability.
3. The PDC magnetron sputtering technique was established at NCAT to produce dielectric coatings such as oxides or nitrides from metallic target materials through the reactive magnetron sputtering process. This process was optimized for PDC depositions of MgO. The optimized parameters for the AJA 1800F system are: gun position of 6 mm, oxygen partial pressure 0.325 mTorr (7.5% in Ar/O_2 mixture), total pressure of 4.3 mTorr, O_2 flow rate of 1.5 sccm, and a frequency of 250 kHz. The

microstructure and preferable orientation of MgO thin films does not depend on power and RF bias. It was found that MgO deposition rates significantly depend on the base water pressure in the deposition chamber. Using the RGA (mass-spectrometer) the threshold base water pressure in the chamber that is necessary for stable PDC depositions of MgO was determined. To achieve repeatable results, the base water pressure in the chamber should not exceed 10^{-8} Torr. Since the water pressure increases during MgO depositions, it is critical to systematically check it and use specific actions to control water pressure in the chamber. Two solutions were developed to decrease the water vapor pressure in the chamber. The first solution was to use a liquid nitrogen cooled water trap ("cold finger") which allows the base pressure to be kept at acceptable low levels. The second solution was to do a short 5-10 minute Mg deposition immediately before an MgO deposition. After these short Mg depositions, there was a drastic drop in the water vapor pressure, down to an acceptable pressure in the 10^{-9}-10^{-8} Torr range. Though this is a very effective way to reduce the water vapor pressure, the first solution is preferable due to the ability to keep the water pressure low and constant for a long time. This also eliminates the need for additional depositions.

4. The corrosion properties of Mg-MgO-Cu multilayers became predictable through its stabilization with a 50 nm thin layer of MgO.
5. X-ray reflectometry was successfully used to measure thicknesses of multilayered coatings.

6. A new optical method was established to evaluate the stability of thin layers of optically transparent oxides. Thin metallic layers of fast corroding metals such as Mg can be used for mimicking substrate materials and as a detector layer for oxide layer degradation. Immersion tests were performed on Mg-MgO systems to evaluate the proposed technique. It was shown that the optical method can be used to obtain resorption rates of coatings and can consequently help to predict resorption times of the coatings as a function of coating thickness. For example, it was shown that MgO dissolves in aqueous media approximately 2.3 times slower than pure metallic Mg in PBS and that the resorption rate of MgO in deionized water was about 3 times lower than in PBS. It also showed that the dissolving process of MgO in aqueous media follows zero order kinetics, therefore, parameters (such as resorption rate) can be used to make quantitative predictions of coating survivability. Immersion tests in different media were also performed at human physiological temperature (37°C). These tests revealed that the behavior of MgO: resorption rates can vary significantly depending on ionic strength, ingredients and biological components (proteins, amino acids, carbohydrates, etc.). For example, the rate in PBS can be up to 15 times slower than in media for cell culturing, and peptides can accelerate and slow down MgO degradation processes depending on the media. These results suggest that, for future tests, extra attention needs to be focused on how the material will perform in the media. This will also give a better understanding of what to expect in the cell adhesion assay and will allow for accurate resorption thickness calculations.

7. Biological test procedures were also established through this study. An increase in power during MgO depositions was implemented in order to increase deposition rates so that reasonable deposition times for desired resorption thicknesses could be achieved. A cell adhesion assay was performed with different thicknesses of MgO and the cells were observed using a phase contrast microscope after a 4 hour incubation period. The most cell adhesion was observed on the control glass substrate with a confluency around 60% and a confluency of around 35% was seen for the thinner 106 and 1122 nm samples. As the MgO thickness increased beyond these two thicknesses, there was little to no cell adhesion. This is most likely due to MgO not degrading completely. In the thinner samples, all the MgO had completely degraded and the cells were able to attach to the glass substrate. Since cell attachment was observed in thinly coated substrates, it can be concluded that MgO was not toxic to the cells. For future tests, different incubation periods will be explored and additional assays, such as live/dead assays, will be performed to further assess the effects of MgO and other materials on cells.

Future work will include the exploration of different galvanic separator materials such as oxides (ZnO, ZrO_2, bioglass) as well as further studies with MgO and nitrides. In continuing the studies of MgO, it is necessary to further optimize deposition parameters in order to achieve more stable coatings and to decrease the porosity in the film. It is also very important to evaluate mechanical properties such as adhesion, hardness, shear strength and abrasive properties for MgO as well as for other prospective oxides in multilayered coatings. Further MgO optimization will lead to more consistent, stable

data. From this study, MgO was proven to be a good galvanic separator material. Through further optimizations and testing, MgO could potentially be a standard for intermediate layers between Mg-based substrates and metallic coatings. In the future, employing this intermediate layer has the potential to create unlimited possibilities for multilayered material combinations because galvanic corrosion between metallic substrates and metallic coatings can be controlled and possibly eliminated. Studying intermediate layers such as MgO will make it possible to one day overcome limitations on materials used in multilayered systems.

REFERENCES

Ahmed, M., & Seifalian, A. M. Organs from nanomaterials. *Handbook of Nanophysics: Nanomedicine and Nanorobotics*, 1-14.

Arnell, R. D., Kelly, P. J., & Bradley, J. W. (2004). Recent developments in pulsed magnetron sputtering. *Surface & Coatings Technology, 188*, 158-163.

Atrens, A., Liu, M., & Abidin, N. I. Z. (2011). Corrosion mechanism applicable to biodegradable magnesium implants. *Materials Science & Engineering B*.

Bandyopadhyay, A., Bernard, S., Xue, W. C., & Bose, S. (2006). Calcium phosphate based resorbable ceramics: Influence of MgO, ZnO, and SiO2 dopants. *Journal of the American Ceramic Society, 89*(9), 2675-2688.

Berg, S., Jonsson, L. B., Nyberg, T., & Katardjiev, I. (2000). Frequency response in pulsed DC reactive sputtering processes. *Thin Solid Films, 365*(1), 43-48.

Binyamin, G., Shafi, B., & Mery, C. (2006). Biomaterials: A primer for surgeons. *Seminars in Pediatric Surgery, 15*, 276- 283.

Brauer, G., Szyszka, B., Vergohl, M., & Bandorf, R. (2010). Magnetron sputtering - Milestones of 30 years. *Vacuum, 84*(12), 1354-1359.

Bruker AXS. (2008). *Diffracplus leptos*. Retrieved September 24, 2011 from http://www.bruker-axs.com/uploads/media/LEPTOS_General_DOC-H88-EXS025_high.pdf.

Bruker AXS. (2011). *D8 discover - new frontiers in the nano-world*. Retrieved September 24, 2011 from http://www.bruker-axs.com/d8_discover.html.

Hitachi High-Technologies. (2008). *Hitachi high-tech launches the su8000*. Retrieved September 24, 2011 from http://www.hitachi-hitec.com/global/whatsnew/2008/20080723.pdf.

Karthikeyan, S., Hill, A. E., Cowpe, J. S., & Pilkington, R. D. (2010). The influence of operating parameters on pulsed D C magnetron sputtering plasma. *Vacuum, 85*(5), 634-638.

Kelly, P. J., & Arnell, R. D. (2000). Magnetron sputtering: a review of recent developments and applications. *Vacuum, 56*(3), 159-172.

Leeuwenburgh, S. C. G., Jansen, J. A., Malda, J., Dhert, W. A., Rouwkema, J., van Blitterswijk, C. A., & Williams, D. F. (2008). Trends in biomaterials research: An analysis of the scientific programme of the World Biomaterials Congress 2008. *Biomaterials, 29*(21), 3047-3052.

Lindtner, R. A., Castellani, C., Hausbrandt, P., Tschegg, E., Stanzl-Tschegg, S. E., Zanoni, G., & Weinberg, A. M. (2011). Bone-implant interface strength and osseointegration: Biodegradable magnesium alloy versus standard titanium control. *Acta Biomaterialia, 7*(1), 432-440.

Luan, B., & Gray, J. E. (2002). Protective coatings on magnesium and its alloys - a critical review. *Journal of Alloys and Compounds, 336*(1-2), 88-113.

Manorama, S. V., Basakand, P., & Singh, S. (2012). Anti-microbial polymer nanocomposites. *Nanocomposite Particles for Bio-Applications*, 249-264.

Mantovani, D., Purnama, A., Hermawan, H., & Couet, J. (2010). Assessing the biocompatibility of degradable metallic materials: State-of-the-art and focus on the potential of genetic regulation. *Acta Biomaterialia, 6*(5), 1800-1807.

Musil, J., Baroch, P., Vlcek, J., Nam, K. H., & Han, J. G. (2005). Reactive magnetron sputtering of thin films: present status and trends. *Thin Solid Films, 475*(1-2), 208-218.

Musil, J., & Vlcek, J. (1999). A perspective of magnetron sputtering in surface engineering. *Surface & Coatings Technology, 112*(1-3), 162-169.

Nie, X., Zhang, P., & Northwood, D. O. (2009). Influence of coating thickness on the galvanic corrosion properties of Mg oxide in an engine coolant. *Surface & Coatings Technology, 203*(20-21), 3271-3277.

Pietak, A. M., Staiger, M. P., Huadmai, J., & Dias, G. (2006). Magnesium and its alloys as orthopedic biomaterials: A review. *Biomaterials, 27*(9), 1728-1734.

Safi, I. (2000). Recent aspects concerning DC reactive magnetron sputtering of thin films: A review. *Surface & Coatings Technology, 127*(2-3), 203-219.

Shastri, V. P. (2006). Future of regenerative medicine: Challenges and hurdles. *Artificial Organs, 30*(10), 828-834.

University at Albany State University of New York. (2011). *Bruker d8 discover*. Retrieved September 24, 2011 from http://cnse.albany.edu/WorldClassResources/MetrologyLabs/AnalyticalCharacterization/Bruker_D8_DISCOVER.aspx.

Welzel, T., Dunger, T., Liebig, B., & Richter, F. (2011). Determination of energy modulations of negative oxygen ions during pulsed magnetron sputtering of magnesium oxide. *Plasma Sources Science & Technology, 20*(3).

Wikipedia. (2011). *Galvanic corrosion*. Retrieved September 15, 2011 from http://en.wikipedia.org/wiki/Galvanic_corrosion.

Wikipedia. (2011). *Profilometer*. Retrieved September 24, 2011 from http://en.wikipedia.org/wiki/Profilometer.

Witte, F. (2010). The history of biodegradable magnesium implants: A review. *Acta Biomaterialia, 6*(5), 1680-1692.

Witte, F., Hort, N., Vogt, C., Cohen, S., Kainer, K. U., Willumeit, R., & Feyerabend, F. (2008). Degradable biomaterials based on magnesium corrosion. *Current Opinion in Solid State & Materials Science, 12*(5-6), 63-72.